

Development of a Yeast-Based Opioid Biosensor by Adaptation of Pheromone Response
Pathway

William Cheney

A Thesis
In the Department of
Biology

Presented in Partial Fulfillment of the Requirements
for the Degree of
Master of Science (Biology)
At Concordia University
Montreal, Quebec, Canada
August 2020
© William Cheney 2020

CONCORDIA UNIVERSITY
School of Graduate Studies

This is to certify that this thesis prepared

By: William Cheney

Entitled: Development of a Yeast-Based Opioid Biosensor by Adaptation of Pheromone Response Pathway

And submitted in partial fulfillment of the requirements for the degree of
Master of Science (Biology)

Complies with the regulations of the University and meets the accepted standard with respect to originality and quality.

Signed by the final Examining Committee:

_____ Chair
Dr. Aashiq Kachroo

_____ Examiner
Dr. Aashiq Kachroo

_____ Examiner
Dr. Christopher Brett

_____ Examiner
Dr. Malcolm Whiteway

_____ Supervisor
Dr. Vincent Martin

Approved by _____
Dr. Selvadurai Dayanandan, Chair of Department

_____ 2020 _____ Dean of Faculty
Dr. Pascale Sicotte

ABSTRACT

Development of a Yeast-Based Opioid Biosensor by Adaptation of Pheromone Response Pathway

William Cheney

Opioids are simultaneously an essential medicine and a leading cause of death. Metabolic engineering and novel opioids offer solutions to insecure supply chains and harmful side effects but are limited by cost and time required for high throughput screening. We have developed a yeast-based opioid biosensor to accelerate opioid research. Utilizing *Homo sapiens* μ -opioid receptor as a detector, our biosensor provides a simulacrum of *in vivo* opioid response while maintaining ease of implementation of a yeast chassis. Functional μ -opioid receptor expression required the introduction of cholesterol biosynthesis as well as pH adjustment. We also identified codon usage as a parameter affecting *Homo sapiens* melatonin receptor1a function and the properties of the μ -opioid receptor binding. Under optimized conditions our opioid biosensor displayed 157-fold increase in fluorescence after opioid exposure and had μ M affinity for opioid peptides and mM affinity for morphine. This opioid biosensor can aid high throughput screening and provides clues for future functional expression of other difficult G-protein coupled receptors.

ACKNOWLEDGEMENTS

I would like to thank my graduate supervisor Vincent Martin for the opportunity to work on this project. It was a fantastic experience I will remember fondly in the future.

I would also like to give huge shout out and thanks to Bjorn Bean for his guidance as well as focusing and refining thoughts, ideas and intuitions.

Another thank you to Malcolm Whiteway who formed the final third of the biweekly dose of wisdom.

Finally, I would like to say thank you to all the past and present Martin lab members: Audrey Morin, Mohamed Nasr, Lauren Narcross, Meghan Davies, Michael Pyne, Nicholas Gold, Mindy Melgar, Leanne Bourgeois, Daniel Tsyplenkov, James Bagley, Kaspar Kevvai, Mathieu Husser, Smita Amarnath, Kealan Exley and Iain Summerby-Murray.

Author Contributions:

Project was conceived by Vincent Martin and Malcolm Whiteway. Dr. Bjorn Bean constructed BBY1580, GFP tagged μ OR and *rne1* Δ . Dr. Bjorn Bean also performed microscopy and image processing of initial μ OR1 localization as well as microscopy of the codon variants of *MTNR1a*. All other work was implemented and analyzed by William Cheney.

Table of Contents

List of Figures.....	VIII
List of Tables	IX
1. Introduction.....	1
1.1 <i>Opioids: long history of use and abuse.....</i>	<i>1</i>
1.2 <i>An opioid biosensor for accelerating research.....</i>	<i>3</i>
1.3 <i>G-protein coupled receptors.....</i>	<i>4</i>
1.4 <i>Opioid receptors.....</i>	<i>5</i>
1.5 <i>Saccharomyces cerevisiae as a biosensor chassis.....</i>	<i>6</i>
1.6 <i>Biosensor design.....</i>	<i>7</i>
2.0 Materials and Methods	9
2.1 <i>Strains and media.....</i>	<i>9</i>
2.2 <i>Plasmids and genes.....</i>	<i>11</i>
2.3 <i>Yeast strain construction.....</i>	<i>13</i>
2.4 <i>Sterol analysis by GC-MS.....</i>	<i>14</i>
2.5 <i>Growth curves.....</i>	<i>14</i>
2.6 <i>Plate reader fluorescence intensity assay.....</i>	<i>15</i>
2.7 <i>Fluorescence microscopy.....</i>	<i>15</i>
2.8 <i>Flow cytometry.....</i>	<i>16</i>
3.0 Results.....	17
3.1 <i>Construction of a cholesterol producing S. cerevisiae strain.....</i>	<i>17</i>
3.2 <i>Biosensor chassis construction.....</i>	<i>20</i>
3.3 <i>Construction and testing of the first generation of biosensor strains.....</i>	<i>21</i>
3.4 <i>Modification of membrane trafficking machinery has no effect H.s.μOR1 localization</i>	<i>23</i>
3.5 <i>Codon usage as a parameter for GPCR function</i>	<i>26</i>
3.6 <i>μOR function is dependent on pH.....</i>	<i>32</i>

3.7 Determination of opioid biosensor's sensitivity.....	34
4.0 Discussion	38
4.1 Biosensor circuit.....	38
4.2 Cholesterol production.....	39
4.3 Effect of codon usage on <i>H. sapiens</i> MTNR1a and OPRM1	40
4.4 Trafficking modulation did not increase plasma membrane localization of <i>H.s.</i> μOR1	42
4.5 Effect of pH on biosensor function.....	42
4.6 Opioids exposure activates biosensor.....	43
4.7 Final remarks.....	44

List of Figures

Figure 1. Structural diversity of opioids..	1
Figure 2. Global opioid production and consumption.....	2
Figure 3. Generalized GPCR activation.....	5
Figure 4. Opioid biosensor schematic.....	8
Figure 5 Sterol biosynthesis.....	17
Figure 6. GC-MS chromatogram of total ion count (TIC) between 12 and 14 min of cholesterol standard (red), ergosterol standard (black), WCY1 (blue), BB1580 (purple) ...	18
Figure 7. Extracted mass spectra from peaks: 1 (cholesterol standard), 2 (Strain WCY1) and 3 (Strain BBY1580) in Figure 6.....	19
Figure 8. Growth profiles for BY4741(black), WCY1(blue) and BBY1580 (purple).....	20
Figure 9. Fold induction of fluorescence for putative biosensors exposed to 10μM of cognate agonist compared to matrix control.....	22
Figure 10. Localization of GFP tagged H.s.μOR1 in wildtype and <i>cne1</i>Δ backgrounds.....	24
Figure 11 Localization of GFP tagged H.s.μOR1 in strains with disrupted AP-1, AP-3 or α-arrestin proteins.....	26
Figure 12 Exponentially weighted average of GC content in GPCR transcripts	29
Figure 13. Effect of codon usage on HsSSTR2 (gray) and HsMTNR1a(salmon) function... 	31
Figure 14. Fluorescence microscopy of codon optimized (top) and native codon (bottom) HsMTNR1a	31
Figure 15. Effect of pH on biosensor activation.....	33
Figure 16 Opioid Biosensor dose response curves	35

List of Tables

Table 1. Strains used in this study	8
Table 2. Plasmids used in this study	11
Table 3. Genes used in this study	11
Table 4. Parameters of dose response curves	35

List of Abbreviations

GPCR: G-protein coupled receptor
GDP: Guanosine diphosphate
GTP: Guanosine triphosphate
GAP: GTPase activating protein
GRK: G-protein coupled receptor kinase
MAPK: Mitogen activated protein kinase
 μ OR: μ (mu)-opioid receptor
H.s μ OR1: *Homo sapiens* μ opioid receptor isoform-I
 κ OR: κ (kappa)-opioid receptor
 δ OR: δ (delta)-opioid receptor
NOP: Nociceptin receptor
YPD: Yeast Peptone Dextrose
SC: Synthetic Complete
OD₆₀₀: Optical Density 600nm
BRET: Bioluminescence resonance energy transfer
ER: Endoplasmic Reticulum
YNB: Yeast nitrogenous base
LiAc: Lithium acetate
GFP: Green fluorescent protein
FI: Fluorescence intensity
PM: Plasma membrane
TIC: Total ion count
w/v: Weight by volume
v/v: Volume by volume
EC50: Half of maximum effective concentration
AU: Arbitrary units
SD: Standard deviation

1. Introduction

1.1 Opioids: long history of use and abuse

Opioids have been used as therapeutics since antiquity¹, yet modern society still struggles to reconcile their costs and benefits. Opioids are a diverse set of compounds (Fig.1) defined by their ability to activate opioid receptors, inducing rapid and potent analgesia. This has made opioids valuable for treatment of pain. Unfortunately, there is a cost to opioid use. Opioids also induce euphoria, a side effect which makes them highly addictive. Finding a way to keep opioids available yet safe will define their place in the 21st century.

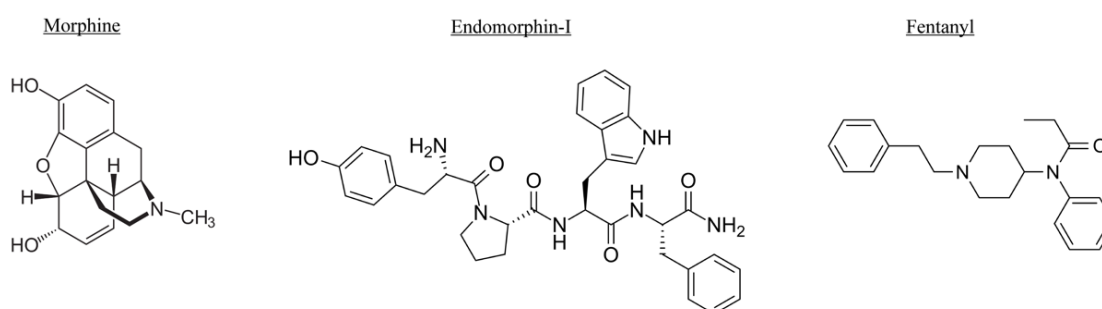


Figure 1. Structural diversity of opioids. A diverse array of compounds activate opioid receptors with varying efficacy. Morphine is a naturally occurring opioid. Endomorphin-I is an endogenous opioid peptide. Fentanyl is a synthetic opioid peptide.

The World Health Organization has classified opioids as an essential medicine for treatment of chronic pain². Opioid supply chains are reliant on *Papaver somniferum* (opium poppy) cultivation for active and precursor compounds. Owing to local regulations and growing conditions, legal *P. somniferum* cultivation is confined to six countries: Australia, France, India, Spain, Turkey and Hungary³. These countries are isolated from consumer markets (Fig. 2) leading to global supply chains with high logistic costs and limited economic integration⁴. Global supply chains are intrinsically vulnerable to disruptions, which could lead to inadequate supply in the United States and Canada which currently have no domestic production.

Metabolic engineering may provide a means to decouple opioid production from *P. somniferum* cultivation by allowing opioid production in other organisms with engineered metabolic pathways⁵. Metabolic engineering has seen success in the production of biofuels⁶ and the antimalarial artemisinin^{7,8}. Biosynthesis of thebaine, a precursor to many opioid compounds, has been shown in *S. cerevisiae*⁹ but high yields remain limited to upstream intermediate (S)-

recticuline¹⁰. Further optimization of the opioid biosynthesis pathway remains necessary, with the cost and speed of screening modified opioid production strains a limiting factor.

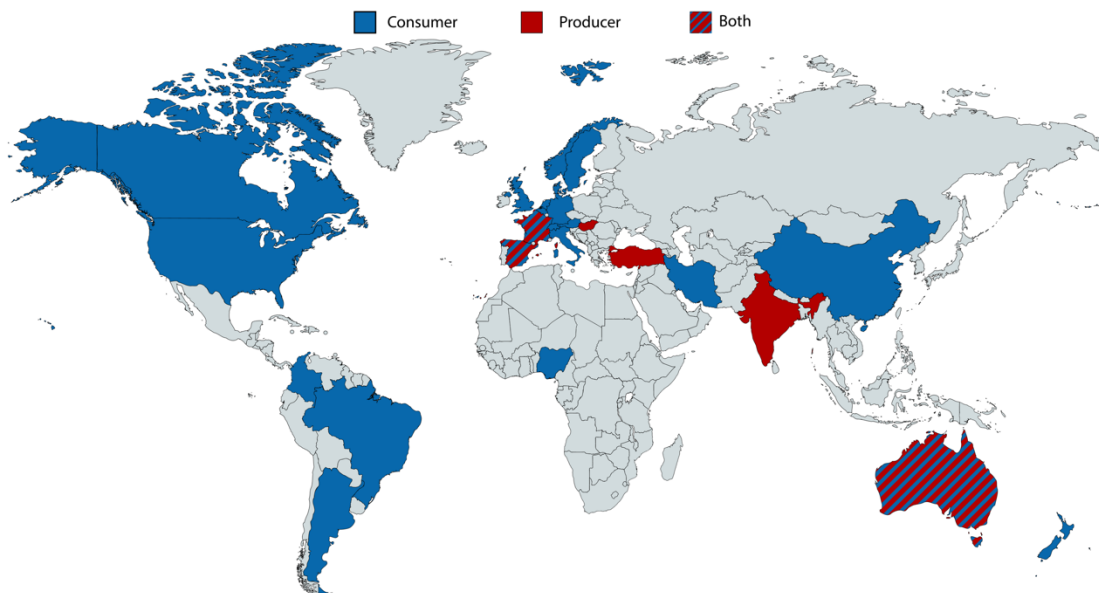


Figure 2. Global opioid production and consumption. Major opioid producers (red) and major opioid consumers (blue) are often geographically distant. Major consumers defined as >1000kg consumed per year.

While opioid production remains fragile, opioid abuse is a more pressing concern. Opioid addiction is serious due to its lethality, which is tied to the wide distribution of opioid receptors across the central, peripheral and enteric nervous system, causing numerous off-target effects^{11,12}. Problematic among these is the combination of addictive euphoria and physical dependence with potentially fatal respiratory depression. Beginning in 1999 over prescription combined with introduction of lab produced synthetic opioids has greatly increased rates of opioid abuse, now referred to as an opioid epidemic¹³. In 2017 opioid overdose accounts for 68% of all overdose deaths and accounted for over 47,000 American deaths in 2017^{14,15}. This crisis has prompted research for better understanding of opioid function and development of novel opioids with diminished side effects.

Opioid properties such as biased agonism have the potential to reduce side effects¹⁶. Biased agonism is the property of an agonist to predominantly activate one of multiple signal transduction pathways. A biased opioid may activate analgesia without respiratory depression. Identification of biased agonism often relies on high-throughput drug screening. Speed, cost and accuracy of these screens again becomes a limiting factor in novel opioid discovery.

1.2 An opioid biosensor for accelerating research

Biosensors make use of biological systems to convert environmental information to observable outputs. Their versatility has led to many applications from landmine detection to cancer diagnosis^{17,18}. Biosensors consist of detector and transducer subsystems. External information enters the system through the detector and is then propagated and converted to an output by the transducer. Organisms have evolved complex systems for detecting and transmitting information¹⁹. These systems can be repurposed as biosensors, and their properties are the primary constraint on biosensor design. Given that opioid receptors represent biological machinery that can detect opioids, the development of an opioid biosensor appears feasible. Such a sensor could accelerate research by decreasing the cost and time of screening novel opioid candidates or opioid production strains²⁰⁻²².

Biosensors are typically composed of either nucleotides or proteins. Nucleotide detectors function by complementary base pairing^{23,24} or aptamer binding²⁵. Transduction is often accomplished through a detector bound probe²⁶, but can also utilize translation to encode any genetically programmable output²⁷. Nucleotide based biosensors are cost-effective but have limited detection capabilities. Current aptamer opioid biosensors offer high sensitivity for target compounds, but likely cannot detect novel opioids or provide mechanistic insight²⁸.

Protein biosensors have greater detection capabilities at the expense of simplicity. Protein biosensors commonly utilize enzymes, transcription factors or receptors each offering unique detection and output possibilities. Enzymatic biosensors provide intrinsic transduction by catalyzing the target information to an output²⁹. Transcription factor biosensors co-opt prokaryotic detection mechanisms to link information detection to gene transcription^{30,31}. Similar to transcription factor, receptor based biosensors adapt eukaryotic information detection to produce desired output^{32,33}. An enzymatic fentanyl biosensor, utilizing transcription factor based transduction, currently exists and again suffers from no potential for novel opioid discovery and limited physiological relevance³⁴.

Incorporating opioid receptors into a biosensor would create a system with greater physiological relevance and novel opioid detection capabilities. This has been done using bioluminescence resonance energy transfer (BRET) between opioid receptors and G-proteins in HEK293 cells³⁵. This system is accurate but is difficult to implement due to its use of

mammalian cells. The challenge remains to functionally express opioid receptors in a tractable system which allows for their effective use as biosensors.

1.3 G-protein coupled receptors

Opioid receptors are members of the G-protein coupled receptor (GPCR) family, which is the largest collection of membrane receptors in humans and facilitates the majority of signal detection/transduction³⁶. All GPCRs share a conserved topology consisting of seven transmembrane α -helices with an extracellular N-terminus and intracellular C-terminus. GPCRs localize to the plasma membrane from which they can bind extracellular signals and transduce the information to downstream signaling machinery.

GPCRs employ a conserved signal transduction mechanism (Fig. 3) involving activation of a physically-associated intracellular G-protein complex^{37,38}. This complex is composed of subunits $G\alpha$, $G\beta$ and $G\gamma$. $G\alpha$ contains a nucleotide binding pocket whose occupancy determines activation state. GDP-bound $G\alpha$ is inactive and associates with a given GPCR through contacts with its intracellular loops and C-terminus. Extracellular agonist binding triggers the propagation of conformational changes through the GPCR, culminating in the GPCR catalyzing exchange of $G\alpha$ GDP for GTP. GTP binding disrupts both $G\alpha$ -GPCR and $G\alpha$ - $G\beta/\gamma$ interactions, causing dissociation of the GPCR, $G\alpha$ and a $G\beta\gamma$ dimer. Both $G\alpha$ and the $G\beta\gamma$ dimer can activate downstream signal transduction. Mammalian genomes encode multiple subtypes of $G\alpha$, $G\beta$ and $G\gamma$ subunits, allowing for specialized response pathways^{37,39}. Signaling is attenuated by GTP hydrolysis on $G\alpha$. $G\alpha$ has intrinsic GTPase activity but with slow reaction kinetics. This reaction is accelerated by a regulator of G-protein signalling protein which functions as a GTPase activating protein (GAP)⁴⁰. GDP bound $G\alpha$ re-sequesters the $G\beta\gamma$ dimer and the reformed complex binds the GPCR.

GPCRs can also activate G-protein independent signal transduction through β -arrestins. β -arrestins facilitate GPCR desensitization by internalization^{38,41}. Prolonged GPCR activation results in phosphorylation of the GPCR's C-terminus by G-protein coupled receptor kinases (GRKs)⁴². β -arrestins bind to this phosphorylated receptor state. This blocks G-protein binding which attenuates their signaling. GPCR bound β -arrestin acts as a scaffold for mitogen activated protein kinases (MAPKs) facilitating their activation^{43,44}. Activated MAPKs are effectors for

signal transduction. In mammals β -arrestin also facilitates receptor endocytosis through interactions with adapter protein complex-2 and clathrin.

Concentration of cell surface receptors will determine sensitivity and magnitude of response, thus GPCR trafficking provides another layer of signaling regulation. Internalized receptors enter the endosome network from which they can be recycled to the plasma membrane or undergo degradation^{40,45}. This decision defines the length of desensitization and is seemingly determined by the ability of β -arrestin to complex with a GPCR. GPCRs expression is complex and has limited their utilization as biosensors.

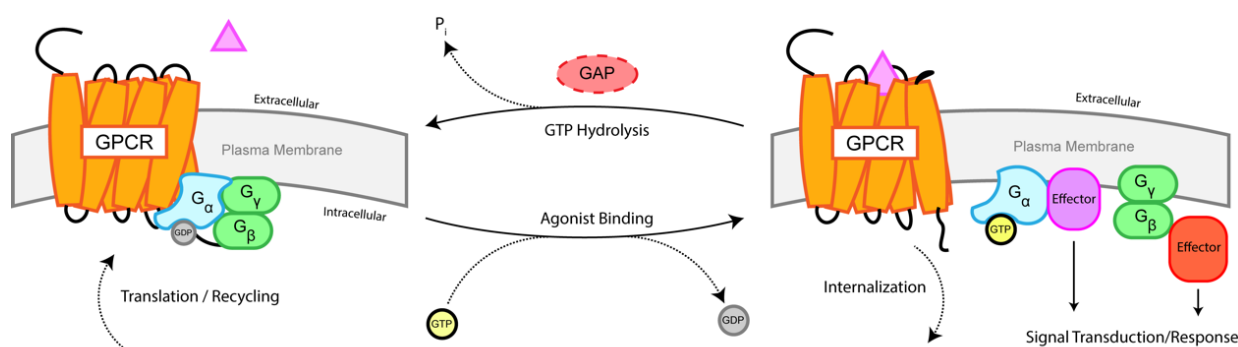


Figure 3. Generalized GPCR activation. Inactive G-protein complex remains bound to the GPCR. Agonist binding results in GTP for GDP exchange on $G\alpha$ and g-protein transition to an active state. In the active state both $G\alpha$ and $G\beta\gamma$ can interact with effectors of signal transduction. GTP hydrolysis on $G\alpha$ reverts transitions the system back to the inactive state. Cell surface receptor population is regulated by rates of production, recycling and internalization

1.4 Opioid receptors

Opioid receptors are divided into four subtypes: μ (μ OR), δ (δ OR), κ (κ OR) and Nociceptin (NOP)^{46–49}. All subtypes have high sequence similarity but have different agonist specificities and distributions, leading to subtype-specific physiological effects^{11,12}. Analgesia and addiction are primarily induced by activation of the μ OR, but can be modulated by secondary activation of δ OR^{50–53}. The mechanism of this modulation is not well elucidated, but possibilities include dimerization or G-protein competition. β -adrenergic receptor antagonist binding also affects analgesia, suggesting modulation can also occur on downstream signaling components⁵⁴. The μ OR is the target for the majority therapeutic opioids and is the focus of most opioid research. This positions the μ OR as the logical detector for an opioid biosensor.

The effect of μ OR activation is cell-type dependent but broadly induces analgesia through ion channel modulation⁵⁵. μ OR can activate both G-protein dependent and/or β -arrestin

dependent signal transduction pathways. μ OR couples through $G\alpha_{i/o}$ subtype, which upon activation inhibits adenylyl cyclase lowering levels of the prominent secondary messenger cAMP affecting cAMP-dependent ion channels^{56,57}. Active $G\alpha_{i/o}$ also activates G-protein gated inward rectifying potassium channel $K_{ir}3$ ^{58,59}. Active $G\beta\gamma$ dimer rapidly inhibits specific calcium ion channels^{60,61}. The net effect of this channel modulation is a decrease in neuronal excitability. Prolonged activation of μ OR results in its phosphorylation by either GRKs or protein kinase C depending on agonist, and allows β -arrestin signalling^{62,63}. Phosphorylated μ OR can bind β -arrestin1/2 and can activate a MAPK ERK1/2 cascade as an alternate signal transduction pathway^{64,65}. Downstream mechanism of this pathway is currently unknown but has effects on opioid tolerance and respiratory depression^{66,67}. With side effects of tolerance and respiratory depression stemming from β -arrestin activation, there is interest in developing biased opioids which preferentially activate G-protein signal transduction. Coupling μ OR activation to an observable output will aid potential drug screens.

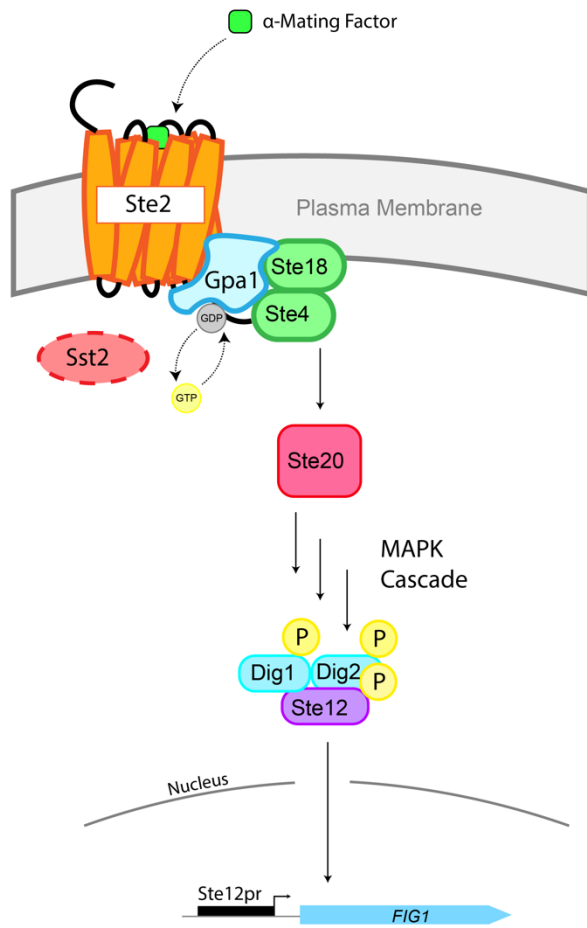
1.5 Saccharomyces cerevisiae as a biosensor chassis.

Saccharomyces cerevisiae has seen steady use as a platform for heterologous GPCR expression^{33,68–70}. *S. cerevisiae* is well characterized, genetically tractable and has required machinery for GPCR expression and signal transduction. More importantly one of *S. cerevisiae* native GPCR circuits, mating response, can be adapted for signal transduction with heterologous GPCRs^{70,71}. These properties have led to the creation of GPCR based fungal pathogen and odorant biosensors, and makes it an ideal chassis for an opioid biosensor^{33,72}. While μ OR has been expressed in *S. cerevisiae*, yeast lacks cholesterol required for *in vivo* function^{73–75}. Specifically, function was restored to μ OR in isolated *S. cerevisiae* membranes by depletion of native sterol ergosterol and addition of cholesterol. Recent work has shown successful introduction of cholesterol biosynthesis in *S. cerevisiae*, potentially opening the door to functional *in vivo* μ OR expression^{74,76}. By combining previous work heterologous GPCR signal transduction with cholesterol biosynthesis we will attempt to build an opioid biosensor in *S. cerevisiae*.

1.6 Biosensor design

The objective of this work is to generate an opioid biosensor in *S. cerevisiae*. Opioid detection will be accomplished by functional expression of *Homo sapiens* μ OR isoform 1 (*H.s.* μ OR1). *H.s.* μ OR1 function is dependent on the presence of cholesterol, therefore making it necessary to introduce cholesterol biosynthesis in place of ergosterol. For mating pathway coupling, it was previously shown that modification of five C-terminal residues of native G protein, Gpa1, to *Homo sapiens* $G\alpha$ residues was sufficient to enable *H.s.* GPCR coupling and activation⁷⁰. To enable *H.s.* μ OR1 coupling and signal transduction Gpa1 will be modified such that its five C-terminal residues, “KIGII” are converted to *H.s.* μ OR1 cognate $G\alpha$, $G\alpha_{i3}$ “ECGLY”⁷⁷. The endogenous yeast mating response activates gene expression through phosphorylation of Dig1, Dig2 and transcription factor Ste12. Dig1 and Dig2 repress Ste12 activity with repression removed through phosphorylation, freeing Ste12 to activate gene transcription. A green fluorescent protein (GFP) reporter will be integrated downstream of a Ste12-activated promoter, coupling mating pathway activation to GFP expression. Sst2 is the endogenous GTPase activating protein for Gpa1 and suppresses signaling, its deletion should improve biosensor sensitivity⁷⁸. Ste2 the endogenous GPCR for mating response will also be deleted as it may compete with *H.s.* μ OR1 for the Gpa1- $G\alpha_{i3}$ chimera, potentially limiting maximal activation.

Native Mating Response Pathway



Modified Mating Response Pathway

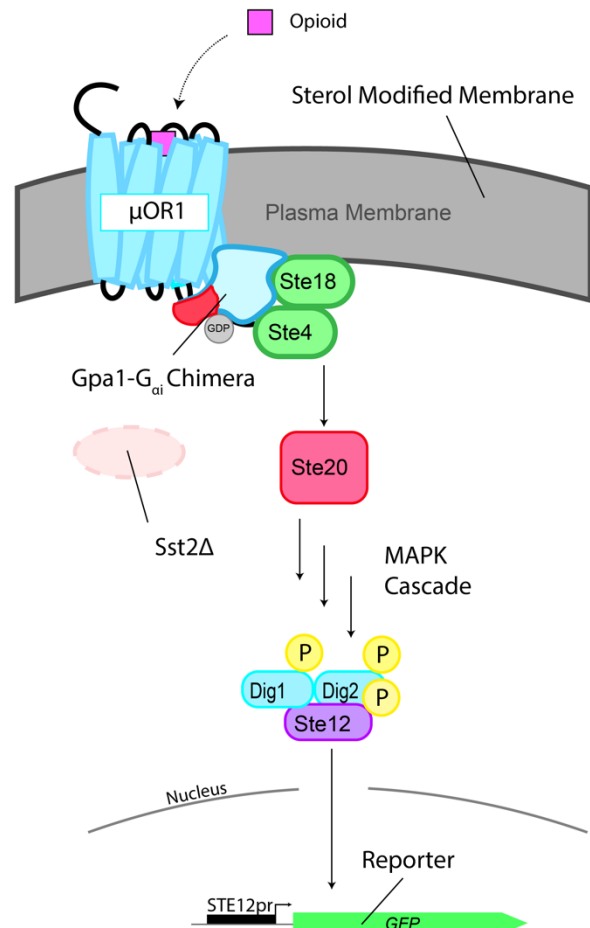


Figure 4. Opioid biosensor schematic. Left: Native mating response pathway. Right: Adapted pathway for opioid detection.

2.0 Materials and Methods

2.1 Strains and media

BY4741(MATa his3Δ1 leu2Δ0 met15Δ0 ura3Δ0) was used as base strain from which all strains were derived. Yeast strains were grown at 30° C while shaking at 200 rpm. Strains were grown on either yeast peptone dextrose (YPD), 10 g L⁻¹ Bacto Yeast Extract, 20 g L⁻¹ Bacto peptone, 20 g L⁻¹ glucose, for transformation and sterol analysis, or synthetic complete media (SC), 6.8 g/L Yeast Nitrogen Base (YNB) with amino acids and supplemented with 2% (w/v) glucose, for flow cytometry and fluorescent intensity assays. Transformed cells were plated on YPD-agar with 200 μg/ml hygromycin and G418 for plasmid selection. All strains used in this study are described in Table 1.

Table 1. Strains used in this study.

Group	Name	Genotype	Source
Cholesterol Biosynthesis	WCY0	<i>erg5Δ, erg6Δ, [FF20]::TDH3p-HsDHCR7-CYC1t, [USERX II-2]::CCW12p-HsDHCR24-PGI1t</i>	This study
	WCY1	<i>erg5Δ, erg6Δ, [FF20]TDH3p-HsDHCR7-CYC1t, [USERX II-2]CCW12p-HsDHCR24-PGI1t, [FF19]TDH3p-DrDHCR7-CYC1t</i>	This study
	BBY1580	<i>[erg6Δ]::TDH3p-DrDHCR24, [erg5Δ]::TDH3p-DrDHCR7</i>	This study
Biosensor Chassis v.1	WCY17	<i>sst2Δ, [fig1Δ]::ENVY, [FF16]::TDH3p-Landing Pad gRNA Target 9-TDH1t GPA1(468-472Δ)-GNAI3(350-354)::URA3</i>	This study
Biosensor v.1	WCY13	<i>erg5Δ, erg6Δ, sst2Δ, [fig1Δ]::ENVY, [FF16]::TDH3p-codon optimized HsOPRM1-TDH1t, GPA1(468-472Δ)-GNAI3(350-354)::URA3, [USERX II-II]CCW12p-HsDHCR24-PGI1t, [FF19]TDH3p-DrDHCR7-CYC1t</i>	This study
	WCY30	<i>ste2Δ erg5Δ sst2Δ [fig1Δ]::ENVY, [FF16]::TDH3p-codon optimized DrOPRM1-TDH1t, GPA1(468-472Δ)-GNAI3(350-354)::URA3, [FF19]::CCW12p-DrDHCR7-TDH1t, [USERXII-2]::CCW12p-HsDHCR24-CYC1t</i>	This study

WCY31	<i>ste2Δ erg5Δ sst2Δ [fig1Δ]::ENVY, [FF16]::TDH3p-codon optimized RnOPRM1-TDH1t, GPA1(468-472Δ)-GNAI3(350-354)::URA3, [FF19]::CCW12p-DrDHCR7-TDH1t, [USERXII-2]::CCW12p-HsDHCR24-CYC1t</i>	This study
WCY32	<i>ste2Δ erg5Δ sst2Δ [fig1Δ]::ENVY, [FF16]::TDH3p-codon optimized HsOPRM1isoII-TDH1t, GPA1(468-472Δ)-GNAI3(350-354)::URA3, [FF19]::CCW12p-DrDHCR7-TDH1t, [USERXII-2]::CCW12p-HsDHCR24-CYC1t</i>	This study
WCY33	<i>ste2Δ erg5Δ sst2Δ [fig1Δ]::ENVY, [FF16]::TDH3p-codon optimized BtOPRK1-TDH1t, GPA1(468-472Δ)-GNAI3(350-354)::URA3, [FF19]::CCW12p-DrDHCR7-TDH1t, [USERXII-2]::CCW12p-HsDHCR24-CYC1t</i>	This study
WCY34	<i>ste2Δ erg5Δ sst2Δ [fig1Δ]::ENVY, [FF16]::TDH3p-codon optimized RnOPRK1-TDH1t, GPA1(468-472Δ)-GNAI3(350-354)::URA3, [FF19]::CCW12p-DrDHCR7-TDH1t, [USERXII-2]::CCW12p-HsDHCR24-CYC1t</i>	This study
WCY35	<i>ste2Δ erg5Δ sst2Δ [fig1Δ]::ENVY, [FF16]::TDH3p-codon optimized MmOPRK1-TDH1t, GPA1(468-472Δ)-GNAI3(350-354)::URA3, [FF19]::CCW12p-DrDHCR7-TDH1t, [USERXII-2]::CCW12p-HsDHCR24-CYC1t</i>	This study
WCY36	<i>ste2Δ erg5Δ sst2Δ [fig1Δ]::ENVY, [FF16]::TDH3p-codon optimized MmOPRD1-TDH1t, GPA1(468-472Δ)-GNAI3(350-354)::URA3, [FF19]::CCW12p-DrDHCR7-TDH1t, [USERXII-2]::CCW12p-HsDHCR24-CYC1t</i>	This study
WCY37	<i>ste2Δ erg5Δ sst2Δ [fig1Δ]::ENVY, [FF16]::TDH3p-codon optimized RnOPRK1-TDH1t, GPA1(468-472Δ)-GNAI3(350-354)::URA3, [FF19]::CCW12p-DrDHCR7-TDH1t, [USERXII-2]::CCW12p-HsDHCR24-CYC1t</i>	This study
WCY49	<i>sst2Δ [fig1Δ]::ENVY, [FF16]::PGK1p-apre-SST2R-TDH1t GPA1(468-472Δ)-GNAI3(350-354)::URA3</i>	This study
BBY1596	<i>ste2Δ, sst2Δ, [FF16Δ]::PGK1p-MTNR1A-TDH1t, [fig1Δ]::ENVY GPA1(468-472Δ)-GNAI3(350-</i>	This study

		354):: <i>URA3</i>	
	BBY1597	<i>ste2Δ, sst2Δ, [FF16Δ]::PGK1p-MTNR1B-TDH1t, [fig1Δ]::ENVY GPA1(468-472Δ)-GNAi3(350-354)::URA3</i>	This study
Trafficking Mutants	EN60	<i>ecm21Δ::G418, csr2Δ::G418, bsd2Δ, rog3Δ::natMX, rod1Δ, ygr068cΔ, aly2Δ, aly1Δ, ldb19Δ, ylr392cΔ::HIS, his3, ura3, leu2,</i>	Nikko <i>et al</i> ⁷⁹
	WCY82	<i>ecm21Δ::G418, csr2Δ::G418, bsd2Δ, rog3Δ::natMX, rod1Δ, ygr068cΔ, aly2Δ, aly1Δ, ldb19Δ, ylr392cΔ::HIS, his3, ura3, leu2, [FF16]::TDH3p-STE2(1-17)-HsOPRM1i1(12-end)-ENVY-TDH1t</i>	This study
	WCY38	<i>Cne1Δ, apl2Δ, [FF16]::TDH3p-STE2(1-17)-HsOPRM1i1(12-end)-ENVY-TDH1t</i>	This study
	WCY41	<i>Cne1Δ, apl6Δ, [FF16]::TDH3p-STE2(1-17)-HsOPRM1i1(12-end)-ENVY-TDH1t</i>	This study
	WCY81	<i>Cne1Δ, apl6Δ, apl2Δ [FF16]::TDH3p-STE2(1-17)-HsOPRM1i1(12-end)-ENVY-TDH1t</i>	This study
Biosensor Chassis v.2	WCY62	<i>sst2Δ, ste2Δ, [fig1Δ]::ENVY, GPA(468-472Δ)1-GNAI3(350-354)</i>	This study
Biosensors v.2	WCY67	<i>sst2Δ, ste2Δ, [fig1Δ]::ENVY, GPA(468-472Δ)1-GNAI3(350-354) PGK1- HsMTNR1A-TDH1t</i>	This study
	WCY79	<i>sst2Δ, ste2Δ, erg5Δ::DrDHCR7, erg6Δ::DrDHCR24, [fig1Δ]::ENVY, GPA1(468-472Δ)-GNAI3(350-354) , [FF16]::PGK1p-codon optimized HsOPRM1-TDH1t</i>	This study
	WCY80	<i>sst2Δ, ste2Δ, erg5Δ::D.r.DHCR7, erg6Δ::DrDHCR24, [fig1Δ]::ENVY, GPA1(468-472Δ)-GNAI3(350-354) , [FF16]::PGK1p-HsOPRM1-TDH1t</i>	This study

[] Denotes Loci of integration, [xΔ] “x” was deleted during integration. All Strains were derived from BY4741(MATa his3Δ1 leu2Δ0 met15Δ0 ura3Δ0). Specific loci: FF16 (YNRCΔ9), FF19 (YORWΔ22), FF20 (YPRCΔ15)

2.2 Plasmids and genes

All plasmids used in this study are described in Table 2 and were maintained in *E.coli* DH5a. pCas plasmid was purchased from Addgene (plasmid #60847) and subsequently modified

by KanMX removal for Hygromycin resistance. Plasmids were extracted by GeneJET plasmid mini-prep kit (Thermo Fisher Scientific). All synthetic genes used in the study are documented in Table 3. *S. cerevisiae* codon optimized *H. sapiens* *DCHR7*, *H. sapiens* *DHCR24*, *D. rerio* *DHCR7*, *D. rerio* *DHCR24*, *H. sapiens* *OPRM1*, *H. sapiens* *OPRMisoII*, *D. rerio* *OPRM1*, *R. norvegicus* *OPRM1*, *R. norvegicus* *OPRK1*, *B. taurus* *OPRK1* and *M. musculus* *OPRK1* were synthesized by Geneart (Thermo Fisher Scientific). *S. cerevisiae* codon optimized *H. sapiens* *MTNR1A*, *H. sapiens* *MTNR1B* and *H. sapiens* *SSTR2* as well as native codon *H. sapiens* *OPRM1*, *H. sapiens* *MTNR1A* and *H. sapiens* *SSTR2* were synthesized by Twist Bioscience. All DNA PCR amplifications were done with PCR using Phusion High-Fidelity DNA polymerase (Thermo Fisher Scientific). DNA was purified using GeneJET Gel Extraction Kit (Thermo Fisher Scientific).

Table 2. Plasmids used in this study.

Plasmid	Genotype	Source
pBB94 (G418)	<i>TEF1p-KanR-TEF1t, RNR2pr-SpCAS9-NLS sequence-CYC1t, tRNA^{Tyr}-HDV-gRNA scaffold-SNR52t</i>	Martin Lab, Derived from Ryan <i>et al</i> ⁸⁰ Addgene #60847
pBB95 (Hyg v.2)	<i>TEF1pr-HygR-TEF1t, RNR2p- Sp CAS9-NLS-CYC1t, tRNA^{Tyr}-HDVribozyme-gRNA scaffold-SNR52t</i>	Martin Lab, Derived from Ryan <i>et al</i> ⁸⁰ Addgene #60847

Table 3. Genes used in this study.

Species	Gene	Refseq
<i>Homo Sapiens</i>	<i>OPRM1</i>	NG_021208.2 isoform-II: NM_001008504.4
	<i>OPRK</i>	NM_000912.5
	<i>DHCR7</i>	NG_012655.2
	<i>DHCR24</i>	NG_008839.1

	<i>MTNR1a</i>	NM_005958
	<i>MTNR1b</i>	NG_028160.1
	<i>SSTR2</i>	NG_029371.1
<i>Danio rerio</i>	<i>OPRM1</i>	NM_131707.2
	<i>DHCR7</i>	NM_201330.2
	<i>DHCR24</i>	NM_001008645
<i>Rattus norvegicus</i>	<i>OPRM1</i>	NM_001038597.2
	<i>OPRK1</i>	NM_017167.3
	<i>OPRD1</i>	NM_012617.1
<i>Bos taurus</i>	<i>OPRK1</i>	NM_001046480.3
<i>Mus musculus</i>	<i>OPRK1</i>	NM_001204371.1

2.3 Yeast strain construction

Genetics modifications were performed by a CRISPR-Cas9 system with *in vivo* assembly by homology directed repair. pCAS was linearized by 16hr double digest with NotI-HF (New England Biolabs #R3189L) and BsaI-HFv2 (New England Biolabs #R3733L). Linearized pCAS-G418, pCAS-Hyg, guide RNA fragment and repair template were introduced in yeast using LiAc transformation⁸¹. Cells were grown overnight to stationary phase then diluted to an optical density (OD₆₀₀) of 0.15 cells for growth to an OD₆₀₀ of 0.6. Cells were harvested by centrifugation for 5 min at 3800 x g washed once with ddH₂O followed by a wash with 100 mM lithium acetate (LiAc). Cells were suspended in transformation mix (100 µl 50% PEG 3350 (w/v), 5.6 µl 3 M LiAc and 4.4 µl boiled salmon sperm DNA) and transferred to a micro tube containing the following DNA parts: 300 µg pCAS G418, 300 µg pCAS HYG, 600 µg gRNA with variable repair DNA. Cells were incubated for 30 min at 30° C followed by heat shock at

42° C for 30 min. Cells were recovered in 500 µl YPD overnight and plated on appropriate selection after 16 hrs. Deletions are performed by utilizing a repair template with a 23-bp sequence corresponding to a Cas9 cut site, within the gene to be deleted, flanked by homology arms. Upon repair the gene is replaced by the 23-bp Cas9 cut site. All modifications were confirmed by colony PCR and/or sequencing.

2.4 Sterol analysis by GC-MS

Sterol content was measured by GC-MS⁸¹. Cells were grown overnight and back-diluted in the morning to an OD₆₀₀ of 0.15. Cells were grown to an OD₆₀₀ of approximately 0.6. Cells were washed once with ice-cold trichloroacetic acid, transferred to a microcentrifuge tube, weighed, and snap-frozen in liquid nitrogen and stored at -80° C until used.

Frozen cells were suspended in 50 µl of water and transferred to a glass spin cap tube, followed by the addition of 50 µl of methanol, 100 µl of glass beads and 100 µl of chloroform. The solution vortexed for six minutes to lyse the cells. Cell extracts were centrifuged at 100 x g for five minutes and the supernatant transferred to a new tube. This process was repeated with 100 µl of chloroform:methanol (2:1) and supernatants were combined. A volume of 34 µl of 0.034% (w/v) MgCl₂ was added to the combined supernatants, vortexed, centrifuged at 800 x g for 5 min and the aqueous phase was removed. This process was repeated once with 34 µl of 3 M KCl:Methanol (4:1). Repeated twice with an artificial aqueous phase (chloroform:methanol:water, 3:48:47). Twenty µl of the organic phase was then transferred to a GC glass autosampler vial and analyzed by GC-MS. Cholesterol (47127-U) and ergosterol (47130-U) analytical standards were bought from Sigma-Aldrich and diluted in chloroform to desired concentrations for construction of a standard curve. Analysis was done in technical triplicates.

2.5 Growth curves

Cholesterol strain fitness was analyzed by construction of 34hr growth curves. Strains were inoculated and grown in YPD for 16hr at 30°C shaking at 200 rpm. Strains were then back diluted into fresh YPD to an OD₆₀₀ of 0.15 and transferred to microtiter plates. Plates were transferred to SunriseTM plate reader (Tecan Life Science). Strains were grown in the SunriseTM at 30°C while shaking at 300 RPM for 34hrs. OD₅₉₅ measurements were taken every 15min over

the 34hr period. Measurements were done in technical triplicate. Growth curves were constructed in python using matplotlib. Standard deviation at each 15min time point was calculated using NumPy. Significance was calculated using student's t-test.

2.6 Plate reader fluorescence intensity assay

Biosensor fluorescence intensity was measured to assay reporter expression. Strains were inoculated and grown overnight at 30° C in SC medium for 16 hrs. Cells were then back diluted with fresh SC using a constant 1:10 dilution factor and grown for an additional 2 hrs at 30° C at 200 rpm. Cells were then transferred to a microtiter plate containing either agonist or vehicle control (1% DMSO for morphine, 1% EtOh (v/v) for melatonin, 1% ddH₂O (v/v) for somatostatin-14). Morphine was acquired with controlled substances exemption from Toronto research chemicals (#60847). α -mating factor was acquired from Genscript (RP01002). The volume of cells transferred was dependent on desired final concentration of the agonist. Cells were then incubated for 4 hrs at 30°C after which fluorescent intensity and OD₆₀₀ values were measured using a CLARIOstar plus plate reader (BGM LABTECH). All measurements were done in biological triplicate. Significance was calculated using independent student t-test calculated in SciPy using function *scipy.stats.ttest_ind*. Standard deviation was calculated by NumPy function *numpy.std* and was calculated on the set of induced/uninduced replicates. Experiments were performed in technical triplicates.

2.7 Fluorescence microscopy

Log phase yeast were imaged using a Zeiss Axioplan microscope equipped with an Infinity 3 camera and a Ph3 Plan-NEOFLUAR 100x/1.30 oil objective and the Infinity Capture Software. Images were acquired using a 800 ms exposure for *apl2* Δ or *apl6* Δ and 900 ms for combined *apl2* Δ , *apl6* Δ . Images were processed in Adobe Photoshop 2019 CC.

2.8 Flow cytometry

Flow cytometry was also used to assay biosensor activity. Strains were inoculated into pH 7.1 SC medium and grown at 30° C and 200rpm for 16 hrs. Cells were back-diluted 1:10 into pH 7.1 SC medium and grown 2 hrs before transfer to a microtiter plate containing agonist or dH₂O. Cells were then grown for 4 hrs at 30°C and shaking at 200 rpm. Flow cytometry was performed with a BD Accuri™ C6 Plus (BD Biosciences) using the FL1-A filter settings (Excitation 488nm, Emission 533nm, 30nm bandwidth) measuring area of a pulse. Thirty thousand non-gated events were recorded for each sample. The synthetic opioid peptide agonists DAMGO ([D-Ala², N-MePhe⁴, Gly-ol]-enkephalin) was acquired from HelloBio (#HB2409), [Met⁵]-Enkephalin, endomorphin-I and endomorphin-II were acquired from Genscript (#RP10886, #RP10925, #RP10926). pH variation assays were performed in biological triplicate. Dose response assays were performed in biological duplicate. Dose response curves were fit using SciPy. Significance was calculated by student's t-test.

3.0 Results

3.1 Construction of a cholesterol producing *S. cerevisiae* strain

Before biosensor construction, a cholesterol producing yeast was developed to allow sterol and growth profile assessment. Validating the characteristics of a cholesterol-rich strain was a necessary first step as the alteration of sterols, which are fundamental components of the membrane, could cause systemic defects. Conveniently, ergosterol, the dominant yeast sterol, and cholesterol biosynthesis largely proceeds along similar pathways with deviations only in the final steps⁸². These deviations include introduction of a methyl group on C-24 in ergosterol and double bond reduction on C-7 in cholesterol (Fig. 5). The pathways branch at zymosterol, from which there are four reactions to cholesterol: C-24 reduction, C-8 isomerization, C-5 desaturation and C-7 reduction reactions are catalyzed by DHCR24, EBP, SC5DL and DHCR7, respectively, and five reactions from zymosterol to ergosterol: C-24 methyl addition, C-8 isomerization, C-5 desaturation, C-22 desaturation and C24-C28 reduction catalyzed in yeast by Erg2, Erg3, Erg5 and Erg4, respectively. C-8 isomerization and C-5 desaturation are present in both pathways and catalyzed by complementary enzymes^{83,84}. Conversion to cholesterol production is further simplified by Erg4 reduction dependence on methyl addition by Erg6. It is therefore sufficient to convert ergosterol to cholesterol biosynthesis by introduction of cholesterol enzymes DHCR7 and DHCR24 and removal of ergosterol enzymes Erg5 and Erg6.

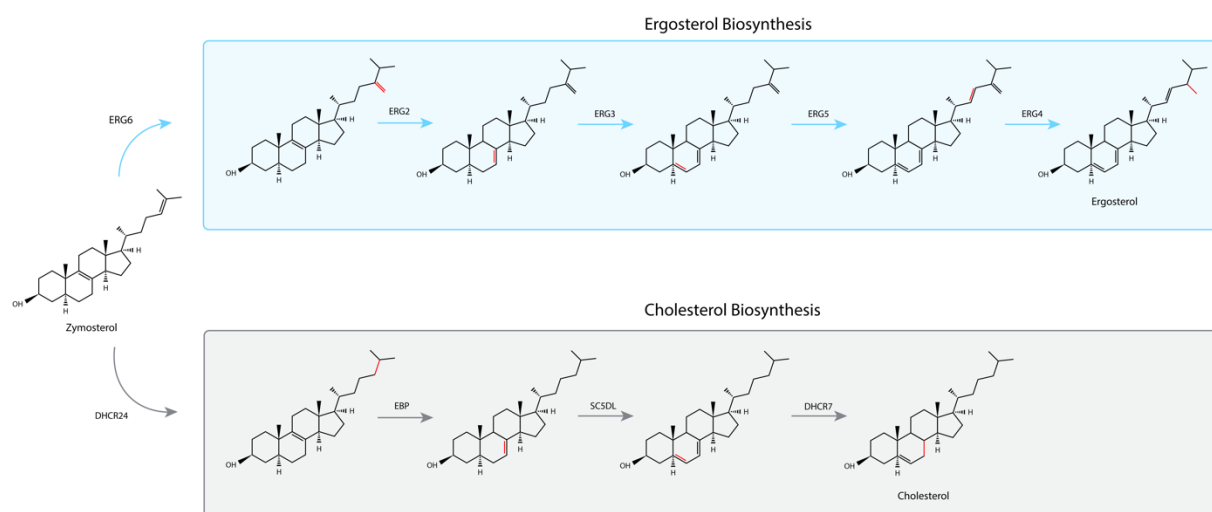


Figure 5 Sterol biosynthesis. Reactions for zymosterol to ergosterol and cholesterol biosynthesis are highly similar with Erg2 and Erg3 being equivalent to EBP and SC5DL. Modification at each step highlighted in red.

Following this blueprint, sterol conversion began with integration of codon optimized *H. sapiens* genes *DHCR7* (*HsDHCR7*) and *DHCR24* (*HsDHCR24*), driven by the strong yeast promoters, into the *S. cerevisiae* genome at safe harbour loci Flagfeldt site 20⁸⁵ and User site XII-2⁸⁶. Subsequently *ERG5* and *ERG6* were deleted to create strain WCY0. Free sterols were isolated using chloroform:methanol extraction and analyzed by gas chromatography mass spectrometry following an established method⁸⁷. Cholesterol and ergosterol were identified by retention time and by comparison of mass spectra to analytical standards. Unexpectedly, WCY0 showed a single peak with a retention time (24.36 min) distinct from both ergosterol and cholesterol (24.174 min) (Supplemental Figure 1A.). Querying the unidentified peak's mass spectra against the NIST database (2.0f Oct. 8, 2008) identified 7-dehydrocholesterol, with a 29.0% match (Supplemental Figure 1B). 7-dehydrocholesterol lacks reduction at C-7 indicating that *HsDHCR7* was not functional. Therefore, a zebrafish ortholog of *DHCR7* (*DrDHCR7*) was introduced at Flagfeldt site 19, to produce strain WCY1. Free sterol analysis of WCY1 revealed a single distinct peak with maximum abundance at retention time 12.66 min, precisely matching the cholesterol standard (Fig. 6). Search of the NIST database returned cholesterol as the top hit with a 36.3% match when queried with the peak's mass spectra which is compared to 31.3% match of the analytical cholesterol standard (Fig. 7).

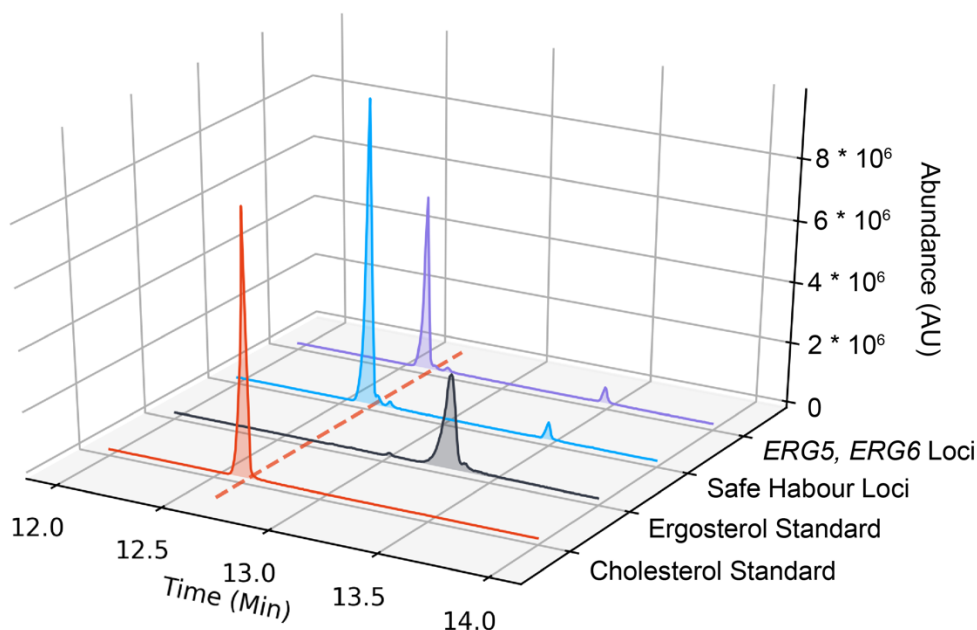


Figure 6. GC-MS chromatogram of total ion count (TIC) between 12 and 14 min of cholesterol standard (red), ergosterol standard (black), WCY1 (blue), BB1580 (purple). Dashed line shows time of maximum value for cholesterol standard. Peak numbers correspond to extracted mass spectra in figure 7. Both WCY1 and BBY1580 have maximum value identical to

cholesterol and distinct from ergosterol. Secondary peak present at approximately 13.50 min in WCY1 and BBY1580 corresponds to internal standard.

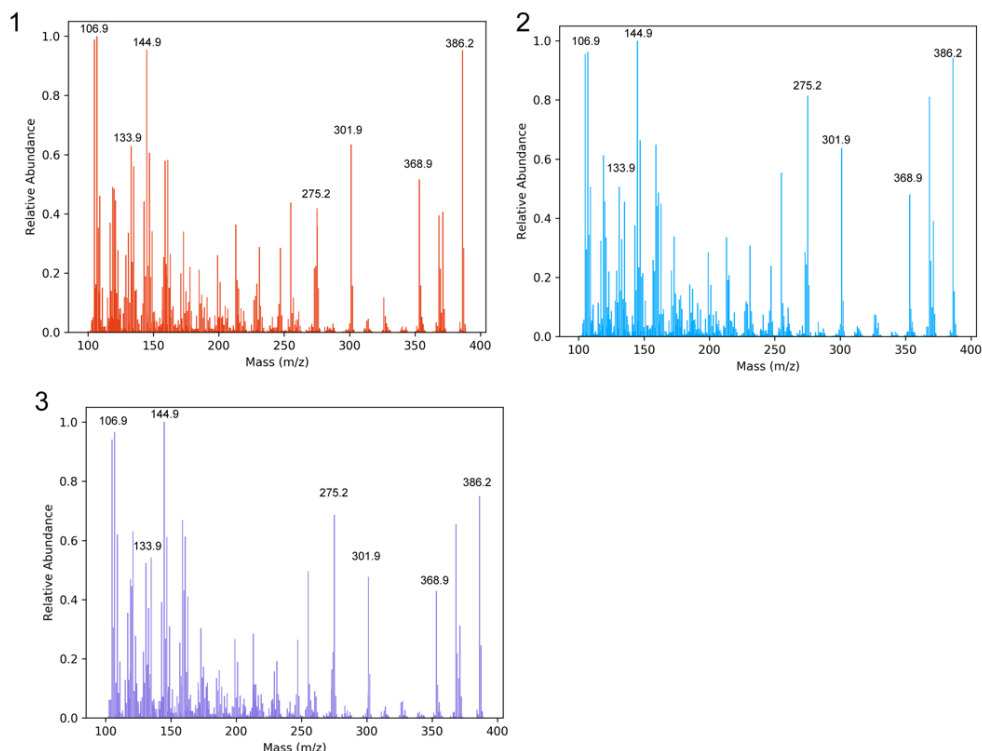


Figure 7. Extracted mass spectra from peaks: 1 (cholesterol standard), 2 (Strain WCY1) and 3 (Strain BBY1580) in Figure 6. Both WCY1 and BBY1580 returned cholesterol when queried against NIST database.

The effect on fitness caused by replacing ergosterol with cholesterol was assessed by tracking growth of wild type and cholesterol-producing (WCY1) yeast over 24 hrs (Fig. 8). WCY1 grew logistically lacking the diauxic shift phase of BY4741. WCY1 displayed a significantly increased lag phase ($p = 7.57 \cdot 10^{-4}$) than BY4741 with a first doubling at approximately 6.5 hours compared to 5 hours for BY4741. To compare growth rates $\partial OD_{600} / \partial T$ was calculated for each time step. The resultant data was very noisy (Supplemental Figure 2), to compensate for this an exponentially weighted average was calculated averaging $\partial OD_{600} / \partial T$ over 1hr (Fig. 8). WCY1 had a similar maximal growth rate as BY4741 (Fig. 8B). WCY1 had significantly ($p = 3.88 \cdot 10^{-3}$) increased duration of high growth rate, $\partial OD_{600} / \partial T \geq 0.0325$, compared to BY4741. Sustained high growth rate compensated for the increased lag phase and WCY1 overtook BY4741 in OD_{600} at approximately 10 hrs. WCY1 growth stops at approximately 1.3 OD_{600} (Fig. 8). While increased maximal growth rate has value in a production environment, a major component of a biosensors value is derived from decreased

iteration times. Ste12 activated gene expression begins within 30min of agonist exposure⁸⁸, adding an additional 2hrs for GFP maturation predicts earliest possible signal detection at 2.5-3hrs. Previous mating pathway biosensors could begin colorimetric detection in a similar time window³³. The prolonged lag phase of WCY1 will limit the total cellular population of the receptor decreasing sensitivity and output during this window. We sought to increase early cellular growth to improve biosensor performance at short assay times.

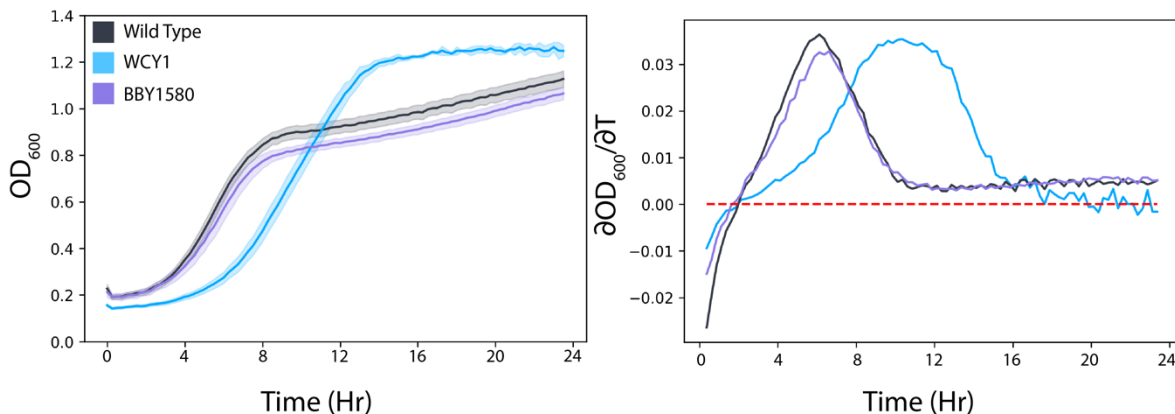


Figure 8. Growth profiles for BY4741(black), WCY1(blue) and BBY1580 (purple). Left: OD₆₀₀ value at 15 min intervals for 24 hours. Shaded area corresponds to \pm SD. Right: Exponentially weighted average of change in OD₆₀₀ at each time step, approximating average change over the previous four timesteps. Dashed line corresponds to $\partial OD_{600}/\partial T = 0$

Given the undesired length of the WCY1 lag phase, we tested placement of *DrDHCR7* and *DrDHCR24* expression cassettes at the *ERG5* and *ERG6* loci respectively, generating BBY1580. Our reasoning was that cis-regulatory elements near the cassettes could help modulate expression improving fitness. Free sterol analysis of BBY1580 identified a single peak with comparable retention time (12.64 min) to cholesterol standard (12.66 min) (Fig. 6). NIST database query returned cholesterol as the top hit (29.8% match) for the peak's mass spectra (Fig 7). Knock-in at ergosterol loci restored wildtype growth pattern with a delineated diauxic shift (Fig. 8A). BBY1580 had a similar first doubling time as BY4741 and growth rates were similar. The decreased lag phase of BBY1580 compared to WCY1 improved its candidacy for a cholesterol chassis. With cholesterol production validated, we began development of the biosensor circuit.

3.2 Biosensor chassis construction

We initially built a chassis containing the desired signal transduction circuit to function as a platform that only requires a heterologous GPCR to be integrated to potentially act as a

biosensor. The signal transduction circuit (Fig. 4) was built by adapting the endogenous pheromone response pathway to accommodate opioid receptors and reporter output. Briefly described, GPCR Ste2 detects external alpha mating factor, leading to activation of cognate G α subunit, Gpa1. Corresponding G β and G γ subunits, Ste4 and Ste18 respectively, activate Ste20 which in turn activates a MAPK cascade. This cascade results in phosphorylation and activation of transcription factor Ste12. Ste12 enters the nucleus and activates gene expression. Observable output was introduced by integration of the GFP variant ENVY downstream of the Ste12-activated promoter *FIG1p*, removing the *FIG1* gene⁸⁹. The *FIG1* promoter has rapid and has among highest fold change relative to other Ste12-activated promoters⁸⁸. The gene encoding a down regulator of the pheromone response pathway, the Gpa1 GTPase *SST2*, was deleted and replaced by a 23-bp Cas9 cut site for potential future targeting. Most heterologous GPCRs have low affinity for *GP1I* binding and activation. To improve affinity between *H.s.* μ OR1 and *GP1I*, a *GP1I*-G α_{i3} chimera was constructed by inserting auxotrophic marker *URA3* downstream of *GP1I*. Homology was designed such that upon *URA3* insertion the five C-terminal residues of *GP1I* are converted to G α_{i3} . G α_{i3} is a cognate G α for *H.s.* μ OR1. Finally, we integrated a “landing pad” into safe harbor loci Flagfledt site 16, which consisted of *TDH3p* and *TDH1t* separated by a previously described 23-bp CAS9 cut site⁹⁰. This landing pad acts to facilitate future insertion of opioid receptors into the chassis. The high strength constitutive promoter *TDH3* was chosen to drive opioid receptor expression as a collision model would predict sensitivity and maximal activation to be concentration dependent^{91,92}. The sum of these modifications resulted in chassis strain WCY17.

3.3 Construction and testing of the first generation of biosensor strains

A complete biosensor strain was assembled by addition of the cholesterol production modifications and a human opioid receptor to the WCY17 chassis strain. A *S. cerevisiae* codon optimized version of human μ OR1 gene, *HsOPRM1*, was integrated into the WCY17 chassis. The 17 N-terminal residues of *H.s.* μ OR1 were converted to Ste2 N-terminal sequence to maintain possible targeting sequence and previously shown to improve expression⁶⁸. This was followed by integration of cholesterol biosynthesis in the safe harbor loci producing the first potential opioid biosensor strain, WCY13.

Biosensor activation was assayed by 4-hr incubation in synthetic complete media with either 10 μ M morphine or 1% (v/v) DMSO as a control. OD₆₀₀-normalized fluorescence intensity (FI) was measured and combined into a single metric FI 10 μ M morphine/FI DMSO (Fold induction of fluorescence) (Fig. 9). The fluorescence of the putative biosensor WCY13 (0.874 ± 0.099 SD) did not increase in the presence of 10 μ M morphine relative to 1% DMSO indicating it was unable to detect the opioid.

To begin troubleshooting the inability of WCY13 to detect morphine, the functionality of the signal transduction pathway and reporter was verified. The biosensor was incubated in synthetic complete media with either 10 μ M α -mating factor, an agonist of the native GPCR Ste2, or a 1%(v/v) dH₂O control. Treatment with 10 μ M alpha-mating factor significantly increased WCY13 fluorescence by over 5 fold relative to the control (5.28 ± 0.351 SD; $p = 1.17 \times 10^{-4}$, assuming null hypothesis of fold induction = 1). This confirmed the integrity of both signal transduction and the reporter, suggesting that the reason WCY13 is unable to detect opioids is a non-functional opioid receptor.

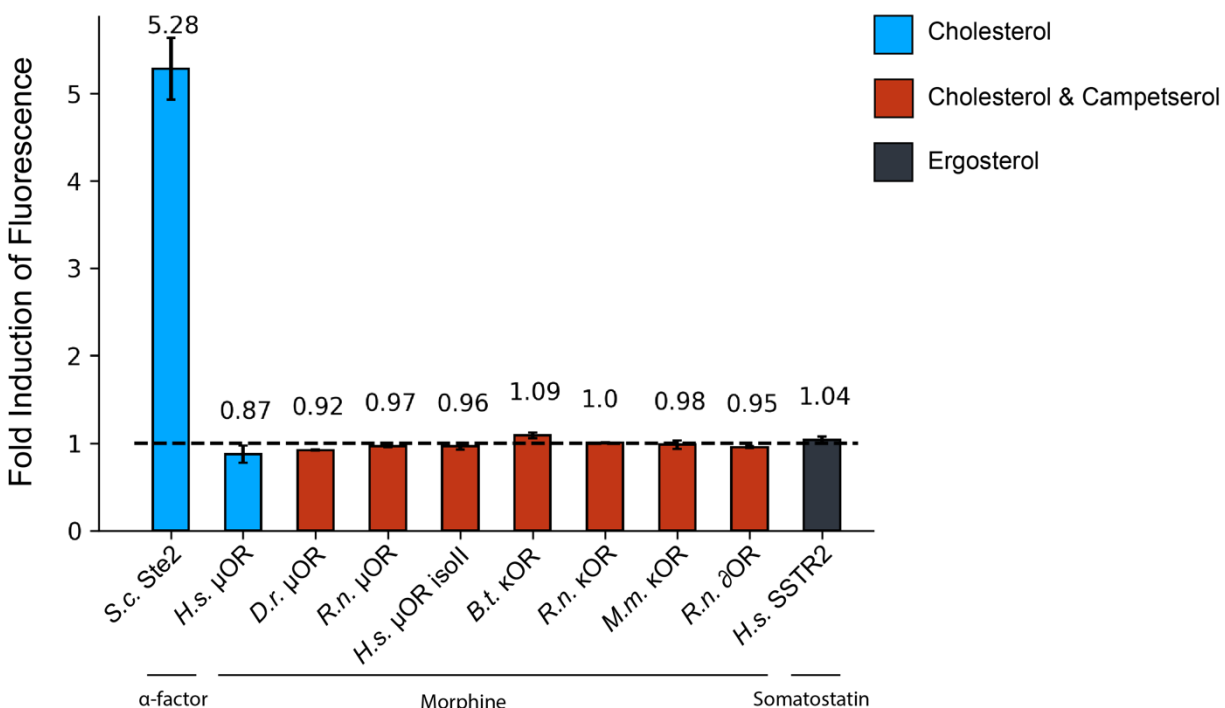


Figure 9. Fold induction of fluorescence for putative biosensors exposed to 10 μ M of cognate agonist compared to matrix control. x axis denotes receptor integrated into the biosensor. Color indicates sterol composition of the strain: cholesterol (blue), cholesterol & campesterol (red) and ergosterol (black). No receptors other than native yeast GPCR Ste2 could induce fluorescence when exposed to agonist. Dashed line corresponds to a fold induction of 1, which indicates no change in fluorescence. Error bars represent \pm SD. * denotes significance compared to a null value of 1.

To explore whether other opioid receptors may be functional in the cholesterol-rich biosensor background we tested an expanded set of yeast codon optimized opioid receptors {*D.renio* μ OR, *R. norvegicus* μ OR, *H. sapiens* μ OR isoformII, *B.taurus* κ OR, *R. norvegicus* κ OR, *M. musculus* κ OR and *R. norvegicus* δ OR} in the WCY17 biosensor chassis. To facilitate strain construction *ERG6* was re-introduced resulting in a “cholesterol-intermediate” strain that produces both cholesterol and campesterol. *STE2* was also deleted in these putative biosensors to prevent competition for the G α chimera. The activity of the resulting array of putative biosensors was again assessed by measuring fluorescence after 4-hr incubation with 10 μ M morphine or 1% DMSO control. All variants failed to respond to morphine with a mean FI 10 μ M morphine/FI DMSO ratio of 0.982 ± 0.049 SD. Failure of a broad spectrum of opioid receptors to activate reporter output implicated additional parameters other than cholesterol were required for function.

As positive controls for the function of exogenous mammalian GPCRs in our background, *H. sapiens* Somatostatin receptor 2(SSTR2) was tested in the WCY17 chassis. SSTR2 had been previously shown as functional, and not dependent on sterol or G α -chimera requirements. Activation assays were performed as above except with 10 μ M of cognate agonist somatostatin-14 substituted for morphine. Concerningly, the SSTR2-based sensor (1.035 ± 0.038 SD) did not respond to 10 μ M somatostatin-14 (Fig 9). Our inability to detect SSTR2 activity suggested that the lack of biosensor function was not opioid receptor-specific, rather there may be systemic problems with the biosensor background, causing GPCR expression or localization issues.

3.4 Modification of membrane trafficking machinery has no effect H.s. μ OR1 localization

To address the possibility that the GPCRs were not properly localized to the plasma membrane, and to gain insight into the cellular machinery that transports them, we expressed C-terminally GFP-tagged *H.s* μ OR1 in wild type yeast. Fluorescence microscopy showed *H.s* μ OR1-GFP predominantly localized to the endoplasmic reticulum (ER) with a smaller vacuolar subpopulation (Fig. 10). The strong ER localization and the lack of a clear population at the plasma membrane (PM) indicated that *H.s.* μ OR1 is largely retained in the ER, possibly due to improper folding or the lack of yeast trafficking signals. In an effort to disrupt the cellular machinery involved in ER retention, facilitating movement of the receptor to plasma membrane,

we deleted *CNE1* and *RER1*, two components of ER quality control likely to play a role in the targeted retention of the GPCRs. *H.s. μOR1* undergoes N-glycosylation and yeast calnexin *CNE1* may be interfering with folding or causing retention⁹³. *RER1* is involved in ER retention of membrane proteins including Ste2⁹⁴. However, deletion of neither *CNE1* nor *RER1* significantly disrupted the ER localization of *H.s μOR1*-GFP, though there may have been a slight increase in vacuolar localization (Fig. 10). This shows that Cne1 and Rer1 do not play a key role in retention, or their functions are redundant with other components of ER quality control.

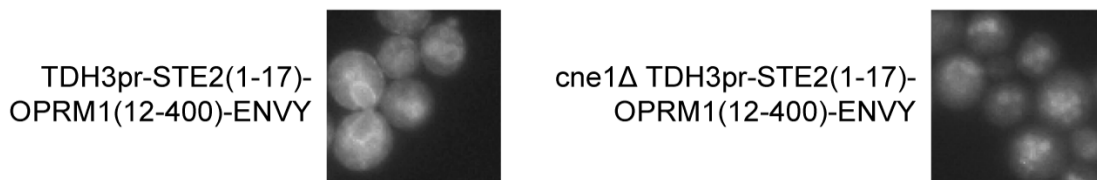


Figure 10. Localization of GFP tagged *H.s.μOR1* in wildtype and *cne1Δ* backgrounds. Both strains show predominant localization to the ER and vacuole, with a potential slight increase to localization present in the *cne1Δ* background. **Strain construction, microscopy and image processing performed by Dr. Bjorn Bean.**

Given the difficulty in disrupting ER retention, we decided to pursue the population of *H.s. μOR1*-GFP that was already escaping the ER by exploring the possibility of redirecting the vacuolar *H.s μOR1*-GFP to the plasma membrane. Movement of *H.s μOR1*-GFP to the vacuole is likely being mediated by at least one of the yeast adapter protein complexes. Adapter protein complexes are each composed of four proteins and facilitate membrane trafficking by driving the formation of vesicles⁹⁵. Yeast adapter protein complex 1 and complex 3 mediate transport between distinct compartments, AP-1 between the Golgi and endosomes and AP-3 from the Golgi to the vacuole⁹⁶⁻⁹⁸. *H.s μOR1*-GFP could be travelling to the vacuole from the Golgi either indirectly via endosomes, using AP-1, or directly, using AP-3. To test if either complex is involved in the vacuolar localization of *H.s μOR1*-GFP, the AP-1 and AP-3 complexes were disrupted by deletion of *APL2* and *APL6* encoding their respective large β subunits. These deletions were performed in the *cne1Δ* background to preserve any possible increase in vacuolar localization. Neither deletion dramatically decreased vacuolar fluorescence (Fig. 11). Deleting both *APL2* and *APL6* together did result in a decreased vacuolar signal, however *H.s μOR1*-GFP was not visible at the plasma membrane. Instead *H.s μOR1*-GFP appeared to accumulate in bright, irregularly shaped ER structures that may have been karmallae, stacks of ER that can form when proteins accumulate at the ER⁹⁹. This ER disfigurement indicated cellular stress,

which would be an increased cost on biosensor function, especially when factoring in cholesterol stress as well.

Though our adaptor protein deletion experiments indicated most vacuolar-targeted *H.s* μ OR1-GFP transits to the vacuole internally and not via the plasma membrane, we attempted to block internalization of any *H.s* μ OR1-GFP that may be reaching the plasma membrane. To do so, we turned to a class of proteins called arrestins that generally link plasma membrane proteins to ubiquitination machinery, triggering internalization. Notably, the endocytosis of the yeast GPCR Ste2 is mediated by α -arrestin proteins^{100,101}. Given their ubiquity and their targeting of at least one GPCR, we reasoned that one of the 13 arrestins may play a role in facilitating internalization of a given exogenous GPCR¹⁰². To test this hypothesis, we took advantage of a strain developed by Nikko *et al.*, and shared by Dr. Chris Brett's lab at Concordia University, that had deletions in 9 arrestins⁷⁹. Addition of *H.s* μ OR1-GFP to this background allowed us to test if any of the 9 arrestins are involved in internalizing *H.s* μ OR1, which would be visible as an apparent increase in plasma membrane fluorescence. However, in this background no plasma membrane signal was detectable, with the ER remaining the dominant localization. Our inability to find trafficking mutations that readily increased the plasma membrane population of *H.s* μ OR1-GFP led us to pursue other ways to improve GPCR function.

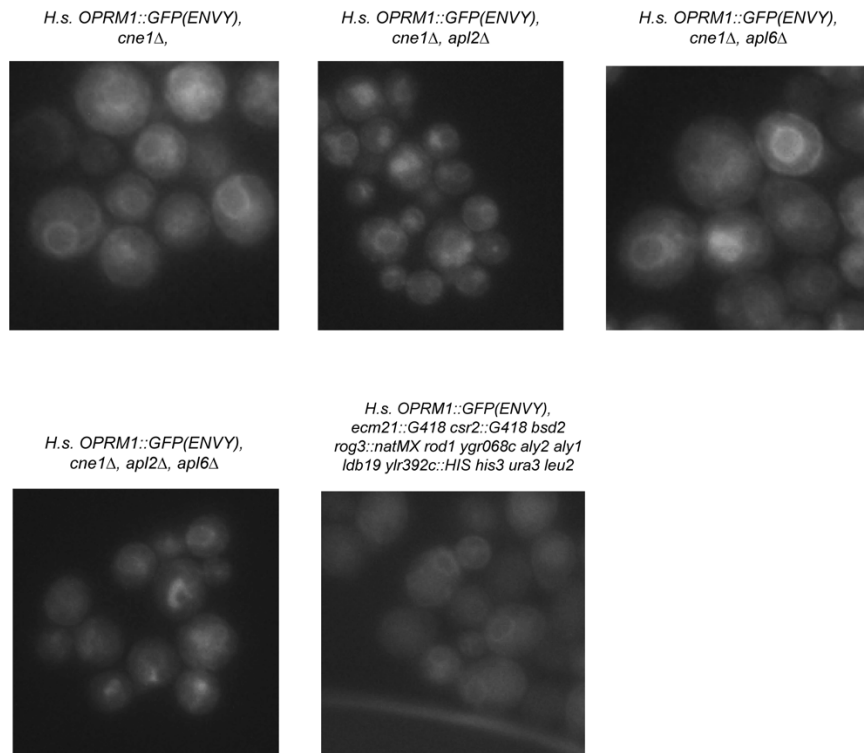


Figure 11 Localization of GFP tagged *H.s.*μOR1 in strains with disrupted AP-1, AP-3 or α-arrestin proteins. There was no discernable increase in plasma membrane localization of *H.s.*μOR1 in any trafficking mutant. AP-1 and AP-3 disruption restricted localization to the ER and resulted in karmallae formation.

3.5 Codon usage as a parameter for GPCR function

Codon optimization is the process of converting a mRNA transcript's codon usage to reflect tRNA abundance in the host organism. This has been shown to increase translation efficiency thereby increasing protein production¹⁰³. However, codon modification inherently disrupts codon position and usage information encoded in the native transcript. Co-translational protein folding allows independent folding of temporally separated domains^{104–106}. Temporal separation is encoded in the mRNA in the form of codon optimality and mRNA secondary structure, can be especially important for α-helix formation and membrane insertion^{107,108}. GPCR folding is complex and difficult even in their native environment¹⁰⁹ and codon usage has been shown to affect *H. sapiens* dopamine receptor D2¹¹⁰. Removing this information by codon optimization may have affected *H.s* μOR1 expression.

Chi square analysis can be used to detect deviation from expected codon usage. Repeated use of a specific codon can deplete its corresponding tRNA pool, slowing translation. Chi square analysis of *H.s.* μ OR1 reveals codon bias for amino acids F ($X^2 = 10.435$, $df = 1$), E ($X^2 = 4.729$, $df = 1$) and C ($X^2 = 5.501$, $df = 1$) compared to *H. sapiens* transcriptome. We next analyzed the position of these biased codons (Supplemental Fig. 4) as clusters of rare codons decrease translation efficiency¹¹¹. Amino acids C or F displayed consistent usage throughout the transcript, while E clustered towards the C-terminus. This may suggest decreasing translation efficiency along transcript due to depletion of C and F tRNA, with further decreases efficiency towards the end of the transcript due to a biased cluster of E codons. These data provide evidence of information encoded within *H.s.* μ OR1's transcript. However, this information has limited use in explaining *H.s.* μ OR1 dysfunction, as codon bias is not maintained between *S. cerevisiae* and *H.s. sapiens* transcriptome. This prompted further investigation into other potential transcript information that would be conserved between species such as mRNA secondary structure.

To identify possible mRNA secondary structure an exponential moving average of GC content was calculated along mRNA transcripts according to equation (1) (Fig. 12), where i is the base pair index, n is the nucleotide at i . The value of θ determines how many base pairs GC content is averaged over. The number of base pairs averaged over is approximately equal to $1/(1 - \theta)$, therefore higher values reduce the effect of local variation. We chose a value of 0.96 for theta which approximates average GC content over 25 base pairs. This value was chosen as it can capture 10-15bp mRNA stem loops while minimizing noise from local variation¹⁵⁰.

$$(1) GC_i = \theta * GC_{(i-1)} + (1 - \theta) * \begin{cases} 1, & n \in \{G, C\} \\ 0, & n \in \{A, T\} \end{cases}$$

Distribution of GC nucleotides in native *H.s. OPRM1*, *H.s. OPRK*, *H.s. MTNR1A*, *H.s. SSTR2*, *R.n. OPRM1*, *S.c. STE2* and codon optimized *H.s. OPRM1* was analyzed. *H.s. OPRM1* (9.23 SD), *H.s. KOR1*(11.27 SD), *R.n. OPRM1* (7.83 SD), *H.s. MTNR1A*(10.64 SD) and *H.s. SSTR2* (8.01 SD) all showed increased variance in GC content than *S.c. STE2*(6.78 SD), indicative of increased local deviation in GC content. As expected the difference in variance was more pronounced when compared to codon optimized *H.s. OPRM1*(4.81 SD) which showed very little variation. All heterologous GPCRs had higher mean GC content than Ste2. With the mean value of each receptor reflecting its native genome. *H. sapiens* receptors have $52.01\% \pm 1.70\%$ mean GC content compared to the mean coding GC content of 52.27% in *H. sapiens*. Ste2 has a

mean GC content of 37.73% compared to 39.77% mean coding GC content in *S. cerevisiae*. *R.n OPRMI* had an mean GC content of 52.38% compared to the 52.59% mean of *R. norvegicus* coding GC content

H.s. OPRMI(bp1-216: 56.63% ± 14.50% SD), *H.s KOR1* (bp1-183: 64.47% ± 19.04% SD), *H.s. MTNR1A*(bp1-90: 57.64% ± 23.05% SD) and *R.n OPRMI*(bp1-205: 55.78% ± 14.05%SD) all showed increased mean GC content in the region between bp 1 and transmembrane helix 1 (TM1) than the mean GC content of the full length transcript. This was inversed in *H.s. SSTR2* with a mean GC content in this region of 41.32% ± 11.60% compared to 51.08% ± 8.01% for the full length transcript. *H.s. OPRMI* (bp 188), *H.s OPRK1*(bp 156), *H.s. MTNR1A* (bp 68) and *R.n OPRMI*(bp 187) had maximal GC content immediately upstream of TM1 start. This early spike was absent in *S.c. STE2*(bp1-150: 33.01% ± 8.50% SD, full length 37.20% ± 6.78 % SD, Max GC index: bp1246) and codon optimized *H.s. OPRMI* (bp1-216: 37.56% ± 9.25% SD, full length: 39.80% ± 4.81% SD, Max GC index: bp111). Increased GC content deviations suggest additional information is present in the native codon transcripts. The GC content spike immediately upstream of TM1 is indicative of mRNA secondary structure and could affect mRNA stability or regulate translational efficiency for proper folding and membrane insertion.

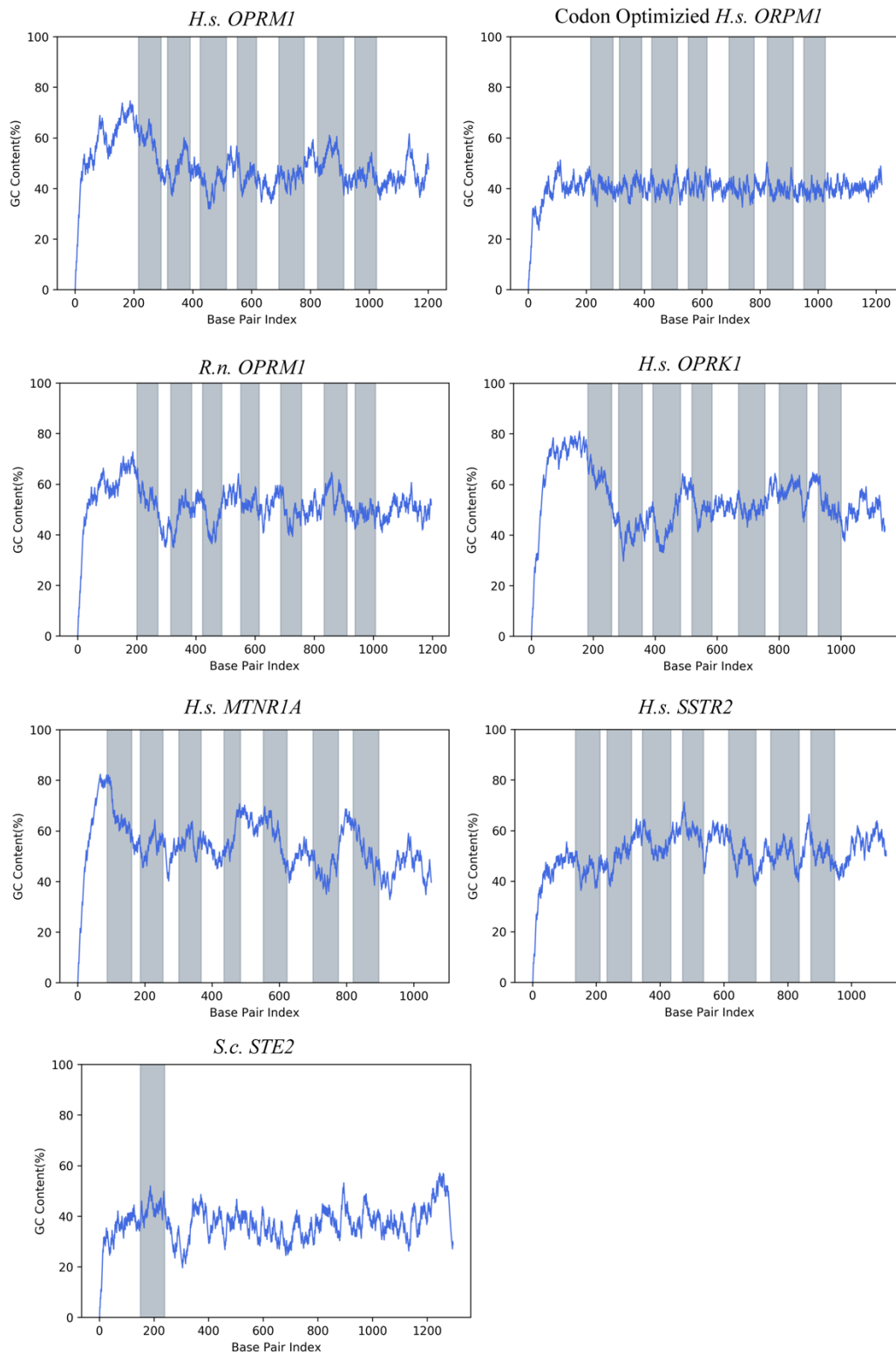


Figure 12 Exponentially weighted average of GC content in GPCR transcripts. GC content was average over the previous 25 base pairs. Shaded regions represent transmembrane helices identified from NCBI annotations. Ste2 was not annotated so only TM1 is shown. *HsOPRM1*, *HsOPRK1*, *HsMTNR1a* and *RnOPRM1* all have maximum GC content immediately before transmembrane helix 1. Codon optimization removed local variation in GC-content.

To experimentally test the effects of codon usage, we introduced *HsMTNR1A*, *HsSSTR2* with native codons into a biosensor chassis. An updated chassis, WCY62, was used that lacks *STE2* and has a marker less integration of GPA1-Ga_{i3} chimera to eliminate potential down regulation by the URA3 marker¹¹². Both native and codon optimized *HsMTNR1A* and *HsSSTR2* biosensor activity was assayed by measuring fluorescence after 4-hr incubation with 10 μM melatonin or somatostatin-14 respectively (Fig. 13). Strikingly, native codons restored the function of *H.s. MTNR1a* (3.67 ± 0.13 SD) showing significant increase ($p = 3.86 * 10^{-5}$) in FI compared to the codon optimized variant (1.13 ± 0.02 SD) but had no effect on *H.s. SSTR2* (Native: 1.036 ± 0.038 SD, Optimized: 1.017 ± 0.014 SD). The assay was repeated with varying concentrations, 10^{-9} M to 10^{-5} M, of melatonin to construct a dose response curve. The Hill equation, equation (2), was fit to the resultant data using SciPy¹¹³.

$$(2) y = a + \frac{(b - a)}{\left(a + \left(\frac{c}{x}\right)^n\right)}$$

Where a is the basal fluorescence intensity, b is maximal fluorescence intensity, c is half of maximal fluorescence intensity (EC50) and n is the hill coefficient. WCY67 had an EC50 of 354 nM and a Hill coefficient of 1.27. This demonstrates that WCY67 can act as melatonin biosensor with an approximately 3.5 fold change in fluorescence after melatonin exposure. This confirms the presence of information encoded within the *HsMTNR1a* transcript, and that this information affects functionality. This proved to be the critical difference between our work and earlier reports of functional expression by Kokkola *et al*¹¹⁴. While the exact mechanism is not elucidated, the GC content spike upstream of TM1 is a noticeable difference between *HsMTNR1a* and *HsSSTR2* transcripts, and may explain why *HsMTNR1a* was affected by codon usage while *HsSSTR2* was not. Microscopy of GFP tagged codon optimized and native codon *HsMTNR1a* showed large difference in expression (Fig. 13). Codon optimized *HsMTNR1a* showed no expression while native codon *HsMTNR1a* showed expression and localization similar to *H.s. μOR1-GFP*. This suggests GC content spike signals mRNA secondary structure and may be critical for mRNA stability similar to *H. sapiens* dopamine receptor D₂. The rescue of *HsMTNR1a* by native codon usage verified the functionality of our biosensor chassis, and prompted us to synthesize *HsOPRM1* with native codon usage and search for other parameters which could affect its expression.

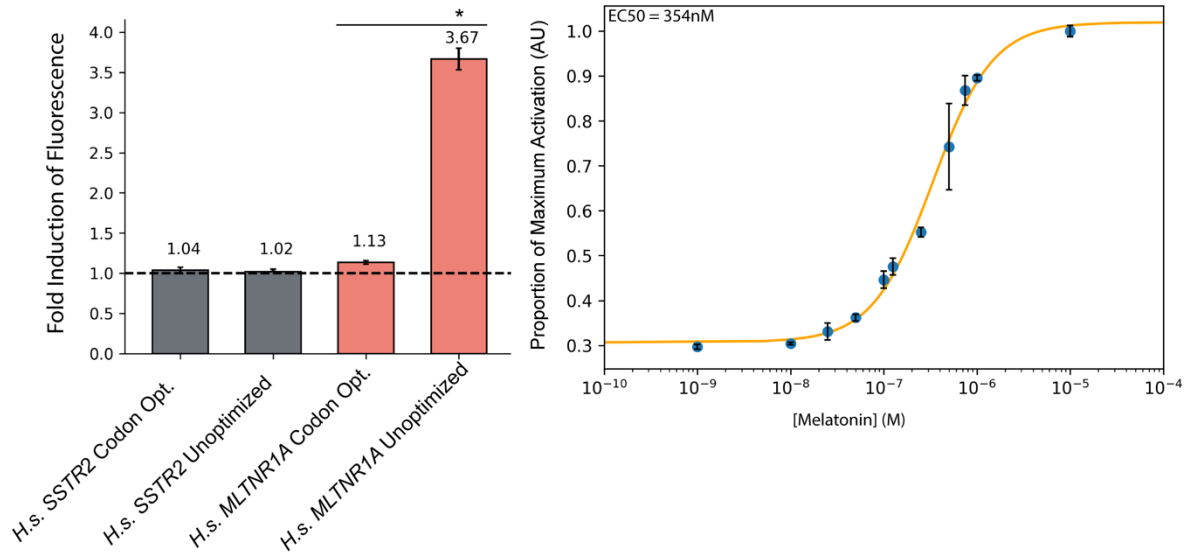


Figure 13. Effect of codon usage on *HsSSTR2* (gray) and *HsMTNR1a* (salmon) function. Left: Fold induction of fluorescence after 4hr exposure to 10 μ M somatostatin or melatonin. Dashed line corresponds to a y value of 1. Error bars represent \pm 1 SD. * denotes significance. Right: Dose response curve of native codon *HsMTNR1a*. Yellow line is curve fit using equation (2). Error bars represent \pm 1 SD.

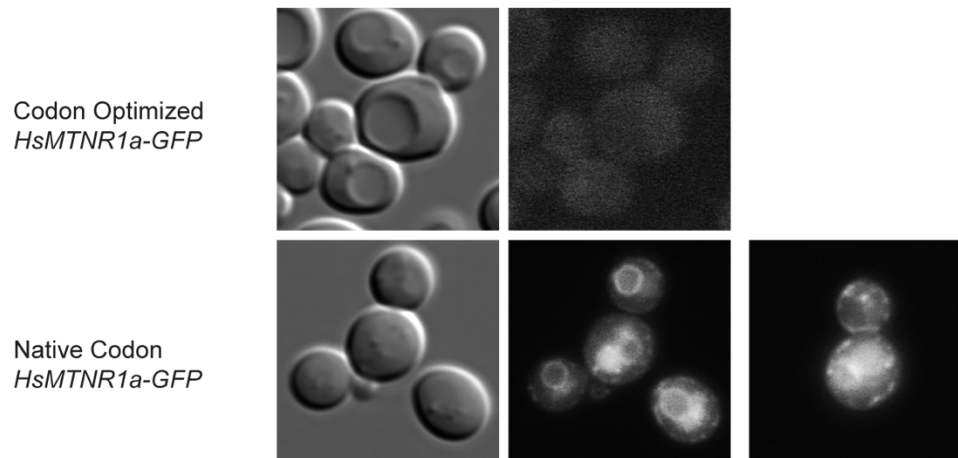


Figure 14. Fluorescence microscopy of codon optimized (top) and native codon (bottom) *HsMTNR1a*. Native codon *MTNR1a* showed expression similar to *HsOPRM1*. Codon optimized *HsMTNR1a* showed no expression. **Strain construction, microscopy and image processing performed by Dr. Bjorn Bean**

3.6 μ OR function is dependent on pH

During our exploration of codon usage, the Gollihar lab at University of Texas at Austin suggested pH may be an important parameter for opioid receptor function. Class A GPCRs have conserved polar interactions that facilitate agonist binding and stabilize the active state of the receptor¹¹⁵⁻¹¹⁷. pH can affect activation in β_2 adrenergic receptor, rhodopsin and there is some evidence of pH affecting opioid receptor function¹¹⁸⁻¹²⁰. The pH of our media (~5.1) was dramatically lower than physiological pH 6.5 - 8.0¹²¹ and is further acidified during growth due to ethanol production.

To evaluate the effect of pH, the response of our original *H.s.* μ OR1-based biosensor, WCY13, to 100 μ M morphine was assayed in media with pH 5.1, 6.1, 7.0 and 8.1. To improve sensitivity and decrease background noise, FI was measured by flow cytometry (Fig. 13). Relative to standard pH 5.1 media there was a significant increase in mean biosensor fluorescence at pH 6.1 (1.6x higher, $p = 1.46 \cdot 10^{-4}$), pH 7 (1.46x higher, $p = 0.002$) and pH 8.1 (1.41x higher, $p = 0.006$). In contrast, the water control displayed an inverse relationship between mean population FI and pH with values decreasing from $1.74 \cdot 10^4$ AU at pH 5.1 to $4.48 \cdot 10^3$ AU at pH 8.1. The population mean FI was significantly increased for 100 μ M morphine exposed biosensor than water control at pH 6.1 ($p = 1.11 \cdot 10^{-4}$), pH 7.0 ($p = 5.28 \cdot 10^{-5}$) and pH 8.1 ($p = 3.58 \cdot 10^{-5}$). Greater differences in population mean FI between morphine and water exposed biosensor was mostly derived from decreases in FI from the ddH₂O exposed biosensor. These results indicate pH as a critical parameter for *H.s.* μ OR1 function. However, biosensor activation by morphine still remained lower than observed with our melatonin biosensor.

Despite morphine's prominence as an analgesic it has weak efficacy for *H.s.* μ OR1 activation compared to other opioid agonists¹³⁰. To explore if other opioids could elicit a stronger response from our biosensor we expanded our set of agonists to include synthetic opioid peptide, D-Ala², N-MePhe⁴, Gly-ol]-enkephalin (DAMGO) and endogenous opioid peptides, [Met⁵]-enkephalin, endomorphin-I and endomorphin-II (Fig. 15). Activation of WCY13 by 100 μ M of each agonist was assayed at each of the above pHs. All these opioid agonists showed greater biosensor activation than morphine at pH 7.0 and 8.1, but with similar activation at pH 5.1. Agonists seemed to induce maximal activation at pH 7.0. Both DAMGO ($p = 2.12 \cdot 10^{-4}$) and endomorphin-II ($p = 0.043$) had significantly greater activation at pH 7.0 than pH 6.1 but had no

significant difference between pH 7.0 and 8.1. [Met⁵]-enkephalin had significantly greater activation at pH 7.0 than pH 6.1 ($p = 0.0012$) or pH 8.1 ($p = 6.69 \times 10^{-4}$). The same trend was observed for endomorphin-I with significantly greater activation at pH 7.0 than pH 6.1 ($p = 2.85 \times 10^{-4}$) or pH 8.1 ($p = 2.15 \times 10^{-3}$). Isolating pH 7.0 data we could compare magnitude of agonist induced activation.

DAMGO induced the greatest activation with significantly greater activation ($p = 1.37 \times 10^{-4}$) than [Met⁵]-enkephalin. There was no significant difference between [Met⁵]-enkephalin and endomorphin-I activation. Both [Met⁵]-enkephalin ($p = 4.39 \times 10^{-5}$) and endomorphin-I ($p = 1.90 \times 10^{-4}$) and had significantly greater activation than endomorphin-II, which in turn had greater activation ($p = 0.0048$) than morphine. These results strengthen the critical role of pH in *H.s* μ OR1 function for our system as pH 5.1 blocks biosensor activation for all agonists. These results also show that morphine is low affinity agonist for our biosensor, when compared to endogenous opioid peptides and DAMGO. DAMGO proved to be the most powerful opioid in our system and showed a 17-fold increase in FI compared to the matrix control validating our biosensors function.

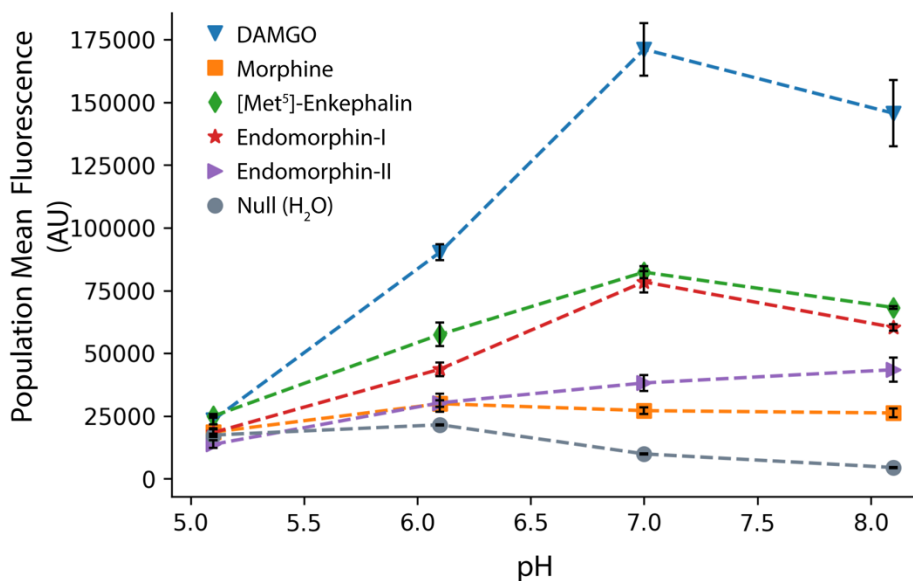


Figure 15. Effect of pH on biosensor activation. Opioid biosensor was exposed to 100 μ M of agonists: DAMGO(blue), [Met⁵]-enkephalin (green), endomorphin-I(red), endomorphin-II(purple), morphine(orange) or matrix control(gray) for four hours, population mean fluorescence was measured by flow cytometry. Biosensor activation was maximal at pH 7.0 or 8.1 depending on agonist. Error bars represent ± 1 SD.

3.7 Determination of opioid biosensor's sensitivity

Determining the sensitivity of our opioid biosensor is critical for its application as a detector and for comparisons to *in vivo* opioid response. Native codon and codon optimized variants of *H.s. OPRM1* were integrated into the updated biosensor chassis, WCY62. Cholesterol genes, *DrDHCR7* and *DrDHCR24* to conserve possible co-evolutionary relationships, were knocked-in at *ERG5* and *ERG6* to produce final biosensor iterations WCY79, codon optimized, and WCY80, native codon. GC-MS analysis confirmed cholesterol as the dominant sterol for both strains. We assayed biosensor activation after 4-hr exposure to 10^{-9} M – 10^{-3} M of opioid agonists: morphine, codeine, DAMGO, [Met⁵] enkephalin, endomorphin-I and endomorphin II. Mean GFP fluorescence (AU) was measured by flow cytometry. Dose response curves were fit to resultant data using equation (2) (Fig. 16).

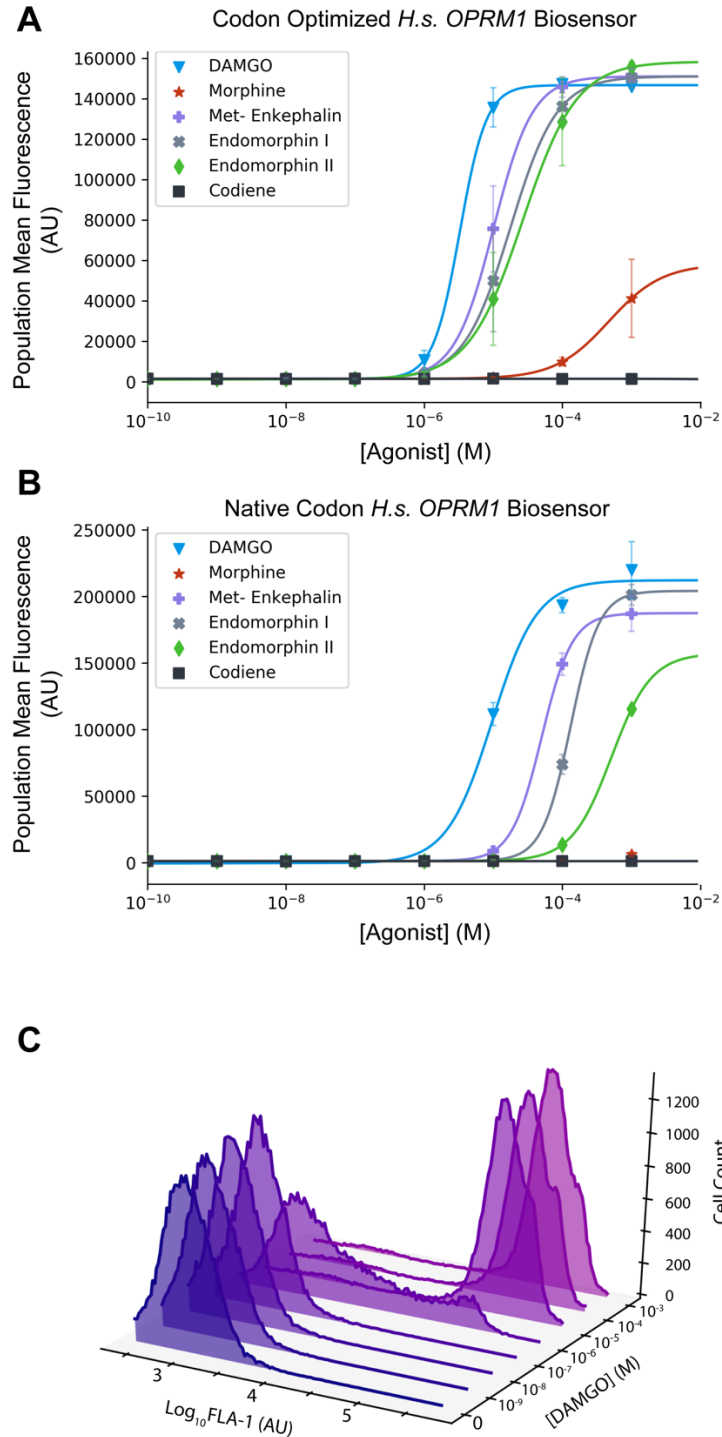


Figure 16 Opioid Biosensor dose response curves. Mean population fluorescence of codon optimized opioid biosensor (A) or native codon opioid biosensor (B) after 4hr exposure to varying concentrations of agonists: DAMGO (blue), [Met⁵]-enkephalin(purple), endomorphin-I(gray), endomorphin-II(green) or codeine (black). Lines represent curve fit using equation (2), Error bars represent ± 1 SD. (C) Representative histogram of cell fluorescence after exposure to varying DAMGO concentrations in codon optimized opioid biosensor.

Both codon optimized, and native codon opioid biosensor showed similar trends in sensitivity (Fig. 14), with agonists ordered by lowest to highest EC50 values: DAMGO, [Met⁵]-enkephalin, endomorphin-I, endomorphin-II and finally morphine. Neither biosensor had any activation by codeine. This trend matches previously reported opioid efficacy and verifies both biosensors behave similarly to *in vivo* response. The codon optimized biosensor showed increased sensitivity than the native codon biosensor for all agonists. This increased sensitivity is likely caused by a higher concentration of cell surface receptor, due to increased translational efficiency, following the law of mass action. Each biosensor showed different relationships between agonists. The native biosensor (199.16 μ M SD) showed increased variance in EC50 between agonists than the codon optimized biosensor (8.70 μ M SD). The native codon biosensor (10281.16 AU) also had increased variance in maximal activation between agonists compared to the codon optimized variant (4177.76 AU). The codon optimized biosensor had significantly lower ($p = 6.71 * 10^{-3}$) maximal activation with only 70% of the native codon biosensor's maximum. There were also significant differences in agonist specific Hill-coefficients (Table 4.), which captures cooperativity of binding. The codon optimized biosensor had a significantly greater ($p = 0.009$) DAMGO Hill-coefficient but significantly smaller ($p = 6.43 * 10^{-4}$, $p = 2.47 * 10^{-6}$, $p = 6.76 * 10^{-4}$) Hill coefficient for [Met⁵]-enkephalin, endomorphin-I and endomorphin-II than the native codon biosensor. Taken together these data show differential agonist efficacy dependent on codon usage. This difference cannot be explained by receptor concentration as that is unidirectional and linear, and instead suggests that codon optimized and native codon *H.s* μ OR1 adopt or exist in different states, which have specific agonist affinity and G-protein activation.

Table 4. Parameters of curves fit in Figure 16.

	<u>Agonist</u>	<u>Basal Activation(a) (AU)</u>	<u>Maximum Activation(b) (AU)</u>	<u>EC 50 (c) (μM)</u>	<u>Hill CoEfficient</u>
<u>Codon Optimized H.s. OPRMI</u>	DAMGO	1302 \pm 292	146675 \pm 414	3.279 \pm 0.07	2.24 \pm 0.04
	[Met ⁵]- Enkephalin	1319 \pm 391	151008 \pm 713	10.14 \pm 0.16	1.54 \pm 0.07
	Endomorphin-I	1174 \pm 233	151010 \pm 550	17.69 \pm 0.28	1.28 \pm 0.02
	Endomorphin-II	989.6 \pm 131	158304 \pm 423	26.65 \pm 0.81	1.11 \pm 0.02
<u>Native Codon H.s. OPRMI</u>	DAMGO	-471.6 \pm 3.91*10 ³	212123 \pm 7.10*10 ³	9.589 \pm 1.2	1.50 \pm 0.33
	Met ⁵]- Enkephalin	1378 \pm 17.4	187442 \pm 39.9	50.22 \pm 0.05	1.96 \pm 2.6*10 ⁻³
	Endomorphin-I	1327 \pm 229	204114 \pm 192	132.0 \pm 0.57	2.10 \pm 0.03
	Endomorphin-II	1313 \pm 25.2	157290 \pm 8.90*10 ³	512.5 \pm 57.6	1.50 \pm 0.06

4.0 Discussion

We developed an opioid biosensor that can accelerate alternative opioid production and novel opioid detection. Utilizing *H. sapiens* μ OR as a detector, our biosensor combines physiological relevance of endogenous opioid detection with an easy to use yeast chassis. These properties give our biosensor increased detection range compared to current enzymatic and nucleotide opioid biosensors^{28,34}, and is easier to implement than current HEK based biosensor³⁵. *S. cerevisiae* was used as a platform for both functional μ -opioid receptor expression and transduction for our biosensor. Functional *H.s* μ OR1 required optimization of known parameters: sterol content, agonist and $G\alpha$ coupling affinity and of new parameters: pH and codon usage. This represents the first *in vivo* expression of functional *H.s* μ OR1 in *S. cerevisiae*. Identification and tuning of these parameters should allow extensive heterologous GPCR expression in *S. cerevisiae* providing a model system for their expression and use of functional GPCRs as a biosensor.

4.1 Biosensor circuit

The *S. cerevisiae* mating response pathway has been extensively used as a transduction circuit for heterologous GPCRs^{33,70,122}. We again validated its efficacy as a signal transduction circuit for *H.s.* μ OR1. Adaptation of the mating response pathway for *H.s.* μ OR1 consisted of four genetic modifications: deletions of *SST2* and *STE2*, construction of *GPA1*- $G\alpha$ Chimera and knock-in of reporter at the *FIG1* loci. While our opioid biosensors utilized *sst2* Δ for improved sensitivity, modulating reaction rate of GTP hydrolysis by *SST2* can tune biosensor sensitivity, valuable for expanding the range of accurately quantifiable concentrations^{122,123}. *Ste2* Δ had no observable effect in our biosensor, as its removal had no effect on maximal activation in our opioid biosensors. This suggests that the population of *GPA1*- $G\alpha$ chimera is greater than the combined *H.s.* μ OR1 and *Ste2* population. The *ste2* Δ modification may have increased impact at higher expression levels of GPCRs where competition for free $G\alpha$ becomes a limiting factor. This circuit can also be used to investigate GPCR- $G\alpha$ interactions. The presence of a potential CAS9 cut site at the 3' end of *GPA1* gene allows modular construction of any *GPA1*- $G\alpha$ chimera. Reporter expression can then be readily applied to assay a GPCR's affinity for specific $G\alpha$ subunits.

While not explored here, a powerful feature of this circuit is dynamic output. Any genetically encodable product can be used as an output. Auxotrophic or antibiotic resistance outputs can link receptor activation to survival thereby creating a tool for artificial selection. This selection could be used to evolve GPCRs to detect alternate signals or for strain optimization^{124,125}. This has advantages over current selection methods which use labeled probes and fluorescence activated cell sorting to select cells with maximal ligand binding. These techniques lack a selection to maintain signal transduction and evolved receptor may not maintain function^{126,127}. Outputs can also encode inputs for secondary GPCR biosensors may allow creation of cellular networks similar to networks found *in vivo*, potentially laying the groundwork for complex computation^{128–130}.

The largest limitation of the *S. cerevisiae* mating circuit is multiple signal integration. Currently there is only one possible output, activation of Ste12 regulated promoters, it is therefore impossible to detect more than one signal without cross talk. Future work to design synthetic signal transduction pathways with scaling dependent only on metabolic constraints is critical to develop intracellular computation. Developing intracellular computation is a necessary precursor to useful cellular computational networks. Intracellular computation in the context of multi-cellular network allows each cell to function as an integrated circuit and facilitates reusability as components are isolated within membranes, abstraction as a specific cell can be used with only input/output information, parallelization as specific cells computation is independent of other cells and finally specialization as each cell metabolic constraints are only dependent on its circuit.

4.2 Cholesterol production

Cholesterol is a known positive allosteric modulator for many class A GPCRs function^{115,131,132}, and was thought to be the primary limitation on opioid receptor function in *S. cerevisiae*⁷³. Building on previous work, we successfully engineered a *S. cerevisiae* strain to produce cholesterol as its dominant sterol (Fig. 6/7). This was achieved through deletion of ergosterol biosynthesis genes *ERG5* and *ERG6* and integration of zebrafish cholesterol biosynthesis genes *D.r. DHCR7* and *D.r. DHCR24*^{74,76}. Two recombinant cholesterol production strains were built differing by integration loci. The first had cholesterol genes integrated at previously described safe harbor loci with subsequent *ERG5* and *ERG6* deletion, While the

second had cholesterol genes integrated at *ERG5* loci and *ERG6* loci. Theoretically safe harbour integration has constant expression dependent on promoter strength, whereas *ERG5/6* loci integration conserves potential local regulatory elements. Both configurations enabled cholesterol production (Fig. 6/7). We observed differential function between *H. sapiens* and *D. rerio* orthologs of *DHCR7*. *H.s. DHCR7* was non-functional, which may be due to additional regulation to control vitamin D biosynthesis¹³³, consistent with this hypothesis fish uptake vitamin D from dietary sources and regulation would be absent on *D.r. DHCR7*¹³⁴. Additional investigation into other *DHCR7* orthologs would be needed to test this hypothesis.

Differences between cholesterol gene expression configurations became apparent in growth assays. While both configurations had lower growth fitness than wildtype, safe harbour integration had logistic growth with extended lag and logistics phases (Fig. 8). *ERG5/6* loci restored wildtype growth phases but at a reduced rate of growth. *ERG5/6* loci also displayed better growth than safe harbour loci until 10 hours. This shows that optimizing cholesterol synthesis can affect fitness. The increased early fitness of *ERG5/6* loci compared to safe harbour loci may be due to ergosterol regulation on these loci separate from limitation on precursors¹³⁵ or could be due to differing ratio in *DHCR7/DHCR24* caused by Ccw12 promoter in the safe harbour strain. The safe harbour loci strain showed 0 growth starting at ~16 hours. This correlates with increased ethanol in the media and the lack of a sustained diauxic shift suggests the cholesterol strains have decreased ethanol tolerance. These data reinforce co-evolutionary relationships between ergosterol and ethanol production, in that ethanol production is toxic for competitors and ergosterol protects from ethanol induced stress reinforcing higher ethanol production, thereby increasing fitness^{136,137}. Longer growth curves will be needed to check if the *ERG5/ERG6* loci strain shares this asymptote. Stress tolerance is complicated in cholesterol strains by loss of function in ergosterol dependent transporters. Notably disruption of weak organic acid transporter Pdr12 could contribute to decreased ethanol tolerance, as well as decreased transformation efficiency⁷⁶. A similar phenotype is observed in *erg6Δ* strain and highlights the importance of methyl on C-24 in divergence between ergosterol and cholesterol¹³⁸.

4.3 Effect of codon usage on *H. sapiens* *MTNR1a* and *OPRM1*

Co-translational folding allows temporally separated protein domains to fold independently of each other, and may be required for correct protein folding or membrane

insertion¹³⁹. This process is dependent on regulating translation efficiency by codon usage and mRNA secondary structure. After initially failing to reproduce previous work, restoring native codon usage rescued *H.s. MTNR1a* function. Analysis of GC-content in GPCR transcripts showed increased local variation in *H. sapiens* GPCRs including maximal GC-content region immediately upstream of transmembrane helix-1 for *MTNR1a*, *H.s. OPRM1* and *H.s. OPRK1*. GC-content is an indicator of mRNA secondary structure due to increased stability of the G/C hydrogen bonding. This secondary structure slows translation efficiency and has been shown to correlate with buried domains such as a GPCR core¹⁴⁰. mRNA secondary structure affects expression of *H. sapiens* dopamine receptor D2 by mRNA stability¹¹⁰. A similar effect could explain codon dependence of *H. sapiens MTNR1a*. Microscopy of GFP tagged MTNR1a showed stark difference in expression between the codon usages. Codon optimized *HsMTNR1a* had no visible expression while native codon *HsMTNR1a* had expression and localization similar to *H.s. μOR1*. This GC-content spike is notably absent for *H. sapiens SSTR2* whose function was unaffected by codon usage. mRNA stability does not explain the effect of codon usage on *H.s. μOR1*, GC-content spike present in *H.s. μOR1* may be required for proper folding and insertion of TM1 into the membrane. Future analysis needs to be done to identify possible codon cluster or codon pairs that also modulate local translation efficiency. *MTNR1a* provides a test environment to investigate how translation efficiency affects function due to its large differential in on/off states. Constructing chimera codon optimized/unoptimized receptors might better elucidate important regions for codon optimization and provide insights into GPCR expression and folding.

While not as binary as MTNR1A, *H.s. μOR1* codon usage affects the properties of the biosensor's dose response curve. The native codon *H.s. μOR1* biosensor had increased variance in maximal activation and EC50 between opioid peptides DAMGO, [Met⁵]-enkephalin, enodomorphin-I and endormorphin-II than codon optimized *H.s. μOR1*. The codon optimized biosensor had higher sensitivity, reflected by lower EC50 values, than the native codon biosensor which could be explained by increased receptor concentration due to translation efficiency. Despite this the native codon biosensor had an increased maximal activation than codon optimized *H.s. μOR*. Codon usage also affects the agonist-specific Hill coefficient. Codon optimized *H.s. μOR* had larger Hill coefficient for DAMGO, while native codon *H.s. μOR* had larger Hill coefficient for [Met⁵]-enkephalin, enodomorphin-I and endormorphin-II. The Hill

coefficient represent cooperativity of agonist binding, with values > 1 indicating positive cooperativity. Cooperativity has been reported at *in vivo* opioid receptors, the mechanism remains unclear but could include dimerization⁵² or multiple G-protein activation^{141–143}. The differing maximal activation and Hill coefficients suggest that native codon *H.s* μ OR1 and codon optimized *H.s* μ OR1 exist in unique conformational states. While the mechanisms remain unclear, we can show the native codon state has increased ability to activate G-proteins as evidenced by higher maximal activation. The native codon state also shows higher cooperativity for endogenous opioid peptides, while the codon optimized state has higher cooperativity for DAMGO.

*4.4 Trafficking modulation did not increase plasma membrane localization of *H.s.* μ OR1*

Biosensor sensitivity is dictated by receptor activation, which is dependent on the concentration of the receptor at the cell surface. Microscopy revealed that *H.s.* μ OR1-GFP largely localizes to the endoplasmic reticulum with a minor vacuolar subpopulation (Fig. 10). Individual attempts to redirect a vacuolar subpopulation to the plasma membrane by deletion of AP-1, AP-3 or arrestin proteins had no effect on *H.s.* μ OR localization. Combination AP-1 and AP-3 deletions limited *H.s.* μ OR to ER at the cost of high cell stress. Subsequent results showed that the predominant ER localization was sufficient for function, raising questions if *H.s.* μ OR1 ER localization is the default state similar to δ OR¹⁴⁴. Fluorescence microscopy will need to be repeated under optimal conditions as cholesterol or pH may affect localization of the receptor. Fluorescence microscopy may lack sensitivity required to detect minor differences in population localization. A biosensor activation assay may provide better insight into the effects of trafficking mutants.

4.5 Effect of pH on biosensor function

Polar interactions and hydrogen bond networks are integral to GPCR agonist binding and signal transduction^{38,117,145}. Our opioid biosensor showed maximal activation at pH 7.0 and 8.1, with minor activation at pH 6.1 and no activation at pH 5.1. Histidine^{6.52} (H299), superscript using Ballesteros-Weinstein numbering¹⁴⁶ which is used to compare residues between GPCRs, is a candidate residue affected by pH. Histidine^{6.52} facilitates hydrogen bonding between *H.s.* μ OR1

and certain agonists, with pH dependent protonation of histidine^{6.52} diminishing binding affinity for these agonists^{147,148}. All opioids in this study hydrogen bond with histidine^{6.52} through their C-terminal hydroxyl group for opioid peptides or C-3 hydroxyl for morphine. Histidine's side chain has a pKa value of ~6, above and below which will affect its capacity for hydrogen bonding¹⁴⁹. *H.s.* μ OR1 had decreased efficacy of hydrogen bonding with agonists at pH 5.1 disrupting receptor activation. Near the pKa of histidine at pH 6.1, *H.s.* μ OR1 had moderate activation consistent with a mixed population of histidine protonation states. Raising the pH of the media to pH 7.0 and 8.1 showed maximal *H.s.* μ OR1 activation, likely due to all receptors having the deprotonated histidine^{6.52} state. Other opioid agonists such as fentanyl do not hydrogen bond with histidine^{6.52}, and could be used to help validate this model. While histidine^{6.52} is specific to opioid receptor binding, agonist binding through polar interactions is conserved in class A GPCRs and pH optimization will be relevant for their functional expression.

4.6 Opioids exposure activates biosensor

Under optimal conditions, cholesterol present and media at pH 7, the codon optimized *H.s.* μ OR1 opioid biosensor had 126-fold increase in population mean FI between on and off states when exposed to opioid peptides, DAMGO, [Met⁵]-enkephalin, endomorphin-I or Endomorphin-II (Fig. 13). Higher fold change was observed for the native codon biosensor which had a maximum of 157-fold increase, raising questions about the effectiveness of codon optimization. The biosensor was weakly activated by morphine and showed no activation by codeine. The biosensor had μ M EC50 values for all opioid peptides, with the greatest affinity for DAMGO followed by [Met⁵]-enkephalin, endomorphin-I and then endomorphin-II. All EC50 values were within one order of magnitude. Depending on agonist the biosensor was 2-3 orders of magnitude less sensitive than *in vivo* opioid receptors which have nM affinity¹⁵⁰. For an opioid biosensor to be useful in drug discovery it should have similar affinities to *in vivo* opioid receptors. *H.s.* μ OR1 activation in HEK293 showed similar agonist affinity order as our biosensor, with DAMGO > [Met⁵]-enkephalin >> endomorphin-I > endomorphin-II > morphine¹⁵⁰. This highlights a limitation of the biosensor in drug discovery, in that morphine's effectiveness as an analgesic is partially orthogonal to μ OR activation, and is instead derived from a lack of internalization and desensitization of μ OR in neurons¹⁵¹. As identifying novel

analgesics is a principle application of our biosensor, improving its detection capabilities may be required for effective use.

Improving biosensor sensitivity is needed for identification of morphine-like compounds and could be accomplished by increasing expression of *H.s* μ OR1 either by increasing promoter strength or copy number. Sensitivity could be further increased with an amplifier circuit where the reporter has positive feedback on itself. As β -arrestin is involved in both negative opioid side effects and receptor endocytosis the introduction β -arrestin signalling will be critical for the identification of novel biased opioids.

4.7 Final remarks

Modern opioids exist in a superposition of two states. In one state, they are an essential medicine with a fragile supply chain and in the other they are a leading cause of death. Better technologies are needed to collapse these states into a secure and effective medicine. Our *H.s* μ OR1 biosensor is a stepping stone for development of opioids and GPCR research and can be readily applied to opioid discovery and metabolic engineering. In the long term this work, by highlighting the positive effect cholesterol production has on mammalian GPCR signaling in yeast, has expanded our ability to express heterologous GPCRs, potentially providing a model system for understanding their complexity.

Reference:

1. Homer. *The Odyssey*, Book IV. pp.221-251. (Palmer T by GH, ed.).
2. *World Health Organization Model List of Essential Medicines, 21st List*. Geneva: World Health Organization; 2019.
3. *International Narcotics Control Board. Estimated World Requirements for 2019 - Statistics for 2017.*; 2019.
4. West G. *Scale: The Universal Laws of Growth, Innovation, Sustainability, and the Pace of Life in Organisms, Cities, Economies and Companies*. Penguin Press; 2017.
5. Stephanopoulos G, Aristidou A, Nielsen J. *Metabolic Engineering*. San Diego: Academic Press; 1998.
6. Atsumi S, Hanai T, Liao JC. Non-fermentative pathways for synthesis of branched-chain higher alcohols as biofuels. *Nature*. 2008;451(7174):86-89. doi:10.1038/nature06450
7. Martin VJJ, Pitera DJ, Withers ST, Newman JD, Keasling JD. Engineering a mevalonate pathway in *Escherichia coli* for production of terpenoids. *Nat Biotechnol*. 2003;21(7):796-802. doi:10.1038/nbt833
8. Ro D-K, Paradise EM, Ouellet M, et al. Production of the antimalarial drug precursor artemisinic acid in engineered yeast. *Nature*. 2006;440(7086):940-943. doi:10.1038/nature04640
9. Galanie S, Thodey K, Trenchard IJ, Filsinger Interrante M, Smolke CD. Complete biosynthesis of opioids in yeast. *Science (80-)*. 2015;349(6252):1095 LP - 1100. doi:10.1126/science.aac9373
10. Pyne ME, Kevvai K, Grewal PS, et al. A yeast platform for high-level synthesis of natural and unnatural tetrahydroisoquinoline alkaloids. *bioRxiv*. January 2019:863506. doi:10.1101/863506
11. Al-Hasani Ph.D. R, Bruchas Ph.D. MR. Molecular Mechanisms of Opioid Receptor-dependent Signaling and Behavior. *Anesthesiol J Am Soc Anesthesiol*. 2011;115(6):1363-1381. doi:10.1097/ALN.0b013e318238bba6
12. Valentino RJ, Volkow ND. Untangling the complexity of opioid receptor function. *Neuropsychopharmacology*. 2018;43(13):2514-2520. doi:10.1038/s41386-018-0225-3
13. (CDC) C for DC and P. Vital signs: overdoses of prescription opioid pain relievers—United States, 1999–2008. *MMWR MorbMortal Wkly Rep 2011 Nov 4*; 2011;60(43):1487-1492.
14. Wilson N, Kariisa M, Seth P, Smith HI, Davis N. Drug and Opioid-Involved Overdose Deaths — United States, 2017–2018. *MMWR Morb Mortal Wkly Rep*. 2020;69:290-297. doi:http://dx.doi.org/10.15585/mmwr.mm6911a4
15. O'Donnell J, Gladden R, Seth P. Trends in Deaths Involving Heroin and Synthetic Opioids Excluding Methadone, and Law Enforcement Drug Product Reports, by Census Region — United States, 2006–2015. *MMWR Morb Mortal Wkly Rep*. 2017;66:897–903. doi:http://dx.doi.org/10.15585/mmwr.mm6634a2External
16. Rankovic Z, Brust TF, Bohn LM. Biased agonism: An emerging paradigm in GPCR drug discovery. *Bioorg Med Chem Lett*. 2016;26(2):241-250. doi:10.1016/j.bmcl.2015.12.024
17. Shemer B, Palevsky N, Yagur-Kroll S, Belkin S. Genetically engineered microorganisms for the detection of explosives' residues. *Front Microbiol*. 2015;6:1175. doi:10.3389/fmicb.2015.01175
18. Tothill IE. Biosensors for cancer markers diagnosis. *Semin Cell Dev Biol*. 2009;20(1):55-

62. doi:<https://doi.org/10.1016/j.semcd.2009.01.015>
19. Hoffman DD. The Interface Theory of Perception. *Stevens' Handb Exp Psychol Cogn Neurosci*. March 2018;1-24. doi:[doi:10.1002/9781119170174.epcn216](https://doi.org/10.1002/9781119170174.epcn216)
 20. DeLoache WC, Russ ZN, Narcross L, Gonzales AM, Martin VJJ, Dueber JE. An enzyme-coupled biosensor enables (S)-reticuline production in yeast from glucose. *Nat Chem Biol*. 2015;11(7):465-471. doi:[10.1038/nchembio.1816](https://doi.org/10.1038/nchembio.1816)
 21. Edmondson R, Broglie JJ, Adcock AF, Yang L. Three-Dimensional Cell Culture Systems and Their Applications in Drug Discovery and Cell-Based Biosensors. *Assay Drug Dev Technol*. 2014;12(4):207-218. doi:[10.1089/adt.2014.573](https://doi.org/10.1089/adt.2014.573)
 22. Keusgen M. Biosensors: new approaches in drug discovery. *Naturwissenschaften*. 2002;89(10):433-444. doi:[10.1007/s00114-002-0358-3](https://doi.org/10.1007/s00114-002-0358-3)
 23. Mikkelsen SR. Electrochemical biosensors for DNA sequence detection. *Electroanalysis*. 1996;8(1):15-19. doi:[10.1002/elan.1140080104](https://doi.org/10.1002/elan.1140080104)
 24. Singh AS and D. Nucleic Acid Based Biosensors for Clinical Applications. *Biosens J*. 2013;2(1):1-8. doi:[10.4172/2090-4967.1000104](https://doi.org/10.4172/2090-4967.1000104)
 25. Lakhin A V, Tarantul VZ, Gening L V. Aptamers: problems, solutions and prospects. *Acta Naturae*. 2013;5(4):34-43.
 26. Sassolas A, Leca-Bouvier BD, Blum LJ. DNA Biosensors and Microarrays. *Chem Rev*. 2008;108(1):109-139. doi:[10.1021/cr0684467](https://doi.org/10.1021/cr0684467)
 27. Green AA, Kim J, Ma D, Silver PA, Collins JJ, Yin P. Complex cellular logic computation using ribocomputing devices. *Nature*. 2017;548(7665):117-121. doi:[10.1038/nature23271](https://doi.org/10.1038/nature23271)
 28. Kammer MN, Kussrow A, Gandhi I, et al. Quantification of Opioids in Urine Using an Aptamer-Based Free-Solution Assay. *Anal Chem*. 2019;91(16):10582-10588. doi:[10.1021/acs.analchem.9b01638](https://doi.org/10.1021/acs.analchem.9b01638)
 29. Robert M, Hicks EC, Renaud-Young, Margaret Mary-Flora Lloyd DC, Oberding LK, George IFS. System and Methods For The Detection of Multiple Chemical Compounds. 2014.
 30. Miller MB, Bassler BL. Quorum Sensing in Bacteria. *Annu Rev Microbiol*. 2001;55(1):165-199. doi:[10.1146/annurev.micro.55.1.165](https://doi.org/10.1146/annurev.micro.55.1.165)
 31. Michener JK, Thodey K, Liang JC, Smolke CD. Applications of genetically-encoded biosensors for the construction and control of biosynthetic pathways. *Metab Eng*. 2012;14(3):212-222. doi:<https://doi.org/10.1016/j.ymben.2011.09.004>
 32. Haider RS, Godbole A, Hoffmann C. To sense or not to sense—new insights from GPCR-based and arrestin-based biosensors. *Curr Opin Cell Biol*. 2019;57:16-24. doi:<https://doi.org/10.1016/j.ceb.2018.10.005>
 33. Ostrov N, Jimenez M, Billerbeck S, et al. A modular yeast biosensor for low-cost point-of-care pathogen detection. *Sci Adv*. 2017;3(6):e1603221. doi:[10.1126/sciadv.1603221](https://doi.org/10.1126/sciadv.1603221)
 34. Bick MJ, Greisen PJ, Morey KJ, et al. Computational design of environmental sensors for the potent opioid fentanyl. *Elife*. 2017;6:e28909. doi:[10.7554/eLife.28909](https://doi.org/10.7554/eLife.28909)
 35. Ehrlich AT, Semache M, Gross F, et al. Biased Signaling of the Mu Opioid Receptor Revealed in Native Neurons. *iScience*. 2019;14:47-57. doi:<https://doi.org/10.1016/j.isci.2019.03.011>
 36. Fredriksson R, Lagerstrom MC, Lundin L-G, Schiöth HB. The G-protein-coupled receptors in the human genome form five main families. Phylogenetic analysis, paralogon groups, and fingerprints. *Mol Pharmacol*. 2003;63(6):1256-1272.

- doi:10.1124/mol.63.6.1256
37. Wettschureck N, Offermanns S. Mammalian G proteins and their cell type specific functions. *Physiol Rev.* 2005;85(4):1159-1204. doi:10.1152/physrev.00003.2005
 38. Rosenbaum DM, Rasmussen SGF, Kobilka BK. The structure and function of G-protein-coupled receptors. *Nature.* 2009;459(7245):356-363. doi:10.1038/nature08144
 39. Flock T, Hauser AS, Lund N, Gloriam DE, Balaji S, Babu MM. Selectivity determinants of GPCR–G-protein binding. *Nature.* 2017;545(7654):317-322. doi:10.1038/nature22070
 40. Magalhaes AC, Dunn H, Ferguson SS. Regulation of GPCR activity, trafficking and localization by GPCR-interacting proteins. *Br J Pharmacol.* 2012;165(6):1717-1736. doi:10.1111/j.1476-5381.2011.01552.x
 41. Kelly E, Bailey CP, Henderson G. Agonist-selective mechanisms of GPCR desensitization. *Br J Pharmacol.* 2008;153 Suppl(Suppl 1):S379-88. doi:10.1038/sj.bjp.0707604
 42. Komolov KE, Benovic JL. G protein-coupled receptor kinases: Past, present and future. *Cell Signal.* 2018;41:17-24. doi:10.1016/j.cellsig.2017.07.004
 43. Jean-Charles P-Y, Kaur S, Shenoy SK. G Protein-Coupled Receptor Signaling Through β -Arrestin-Dependent Mechanisms. *J Cardiovasc Pharmacol.* 2017;70(3):142-158. doi:10.1097/FJC.0000000000000482
 44. Lefkowitz RJ, Shenoy SK. Transduction of receptor signals by beta-arrestins. *Science.* 2005;308(5721):512-517. doi:10.1126/science.1109237
 45. Hanyaloglu AC, von Zastrow M. Regulation of GPCRs by endocytic membrane trafficking and its potential implications. *Annu Rev Pharmacol Toxicol.* 2008;48:537-568. doi:10.1146/annurev.pharmtox.48.113006.094830
 46. Brownstein MJ. A brief history of opiates, opioid peptides, and opioid receptors. *Proc Natl Acad Sci U S A.* 1993;90(12):5391-5393. doi:10.1073/pnas.90.12.5391
 47. Zaveri NT. Nociceptin Opioid Receptor (NOP) as a Therapeutic Target: Progress in Translation from Preclinical Research to Clinical Utility. *J Med Chem.* 2016;59(15):7011-7028. doi:10.1021/acs.jmedchem.5b01499
 48. Waldhoer M, Bartlett SE, Whistler JL. Opioid Receptors. *Annu Rev Biochem.* 2004;73(1):953-990. doi:10.1146/annurev.biochem.73.011303.073940
 49. Matthes HWD, Maldonado R, Simonin F, et al. Loss of morphine-induced analgesia, reward effect and withdrawal symptoms in mice lacking the μ -opioid-receptor gene. *Nature.* 1996;383(6603):819-823. doi:10.1038/383819a0
 50. Wang D, Tawfik VL, Corder G, et al. Functional Divergence of Delta and Mu Opioid Receptor Organization in CNS Pain Circuits. *Neuron.* 2018;98(1):90-108.e5. doi:10.1016/j.neuron.2018.03.002
 51. Schmidt BL, Tambeli CH, Levine JD, Gear RW. μ /delta Cooperativity and opposing kappa-opioid effects in nucleus accumbens-mediated antinociception in the rat. *Eur J Neurosci.* 2002;15(5):861-868. doi:10.1046/j.1460-9568.2002.01915.x
 52. Gomes I, Jordan BA, Gupta A, Rios C, Trapaidze N, Devi LA. G protein coupled receptor dimerization: implications in modulating receptor function. *J Mol Med.* 2001;79(5):226-242. doi:10.1007/s001090100219
 53. Qi J, Mosberg HI, Porreca F. Selective modulation of morphine antinociception, but not development of tolerance, by δ receptor agonists. *Eur J Pharmacol.* 1990;186(1):137-141. doi:https://doi.org/10.1016/0014-2999(90)94071-5
 54. Afify EA, Andijani NM. Potentiation of Morphine-Induced Antinociception by

- Propranolol: The Involvement of Dopamine and GABA Systems. *Front Pharmacol.* 2017;8:794. doi:10.3389/fphar.2017.00794
55. Williams JT, Christie MJ, Manzoni O. Cellular and Synaptic Adaptations Mediating Opioid Dependence. *Physiol Rev.* 2001;81(1):299-343. doi:10.1152/physrev.2001.81.1.299
 56. Ingram SL, Williams JT. Opioid inhibition of I_h via adenylyl cyclase. *Neuron.* 1994. doi:10.1016/0896-6273(94)90468-5
 57. Taussig R, Iniguez-Lluhi JA, Gilman AG. Inhibition of adenylyl cyclase by Gi alpha. *Science (80-).* 1993;261(5118):218 LP - 221. doi:10.1126/science.8327893
 58. North RA, Williams JT, Surprenant A, Christie MJ. Mu and delta receptors belong to a family of receptors that are coupled to potassium channels. *Proc Natl Acad Sci.* 1987;84(15):5487 LP - 5491. doi:10.1073/pnas.84.15.5487
 59. Ippolito DL, Temkin PA, Rogalski SL, Chavkin C. N-terminal Tyrosine Residues within the Potassium Channel Kir3 Modulate GTPase Activity of G α i. *J Biol Chem.* 2002;277(36):32692-32696. doi:10.1074/jbc.M204407200
 60. Wilding TJ, Womack MD, McCleskey EW. Fast, local signal transduction between the mu opioid receptor and Ca²⁺ channels. *J Neurosci.* 1995;15(5 Pt 2):4124-4132.
 61. Bourinet E, Soong TW, Stea A, Snutch TP. Determinants of the G protein-dependent opioid modulation of neuronal calcium channels. *Proc Natl Acad Sci U S A.* 1996;93(4):1486-1491. doi:10.1073/pnas.93.4.1486
 62. Johnson EA, Oldfield S, Braksator E, et al. Agonist-Selective Mechanisms of μ -Opioid Receptor Desensitization in Human Embryonic Kidney 293 Cells. *Mol Pharmacol.* 2006;70(2):676 LP - 685. doi:10.1124/mol.106.022376
 63. Zhang J, Ferguson SSG, Barak LS, et al. Role for G protein-coupled receptor kinase in agonist-specific regulation of μ -opioid receptor responsiveness. *Proc Natl Acad Sci.* 1998;95(12):7157 LP - 7162. doi:10.1073/pnas.95.12.7157
 64. Macey TA, Lowe JD, Chavkin C. Mu opioid receptor activation of ERK1/2 is GRK3 and arrestin dependent in striatal neurons. *J Biol Chem.* 2006;281(45):34515-34524. doi:10.1074/jbc.M604278200
 65. Miyatake M, Rubinstein TJ, McLennan GP, Belcheva MM, Coscia CJ. Inhibition of EGF-induced ERK/MAP kinase-mediated astrocyte proliferation by mu opioids: integration of G protein and beta-arrestin 2-dependent pathways. *J Neurochem.* 2009;110(2):662-674. doi:10.1111/j.1471-4159.2009.06156.x
 66. Kliewer A, Schmiedel F, Sianati S, et al. Phosphorylation-deficient G-protein-biased μ -opioid receptors improve analgesia and diminish tolerance but worsen opioid side effects. *Nat Commun.* 2019;10(1):367. doi:10.1038/s41467-018-08162-1
 67. Zhou L, Bohn LM. Functional selectivity of GPCR signaling in animals. *Curr Opin Cell Biol.* 2014;27:102-108. doi:https://doi.org/10.1016/j.ceb.2013.11.010
 68. King K, Dohlman HG, Thorner J, Caron MG, Lefkowitz RJ. Control of yeast mating signal transduction by a mammalian beta 2-adrenergic receptor and Gs alpha subunit. *Science.* 1990;250(4977):121-123. doi:10.1126/science.2171146
 69. Scott BM, Chen SK, Bhattacharyya N, et al. Coupling of Human Rhodopsin to a Yeast Signaling Pathway Enables Characterization of Mutations Associated with Retinal Disease. *Genetics.* 2019;211(2):597 LP - 615. doi:10.1534/genetics.118.301733
 70. Brown AJ, Dyos SL, Whiteway MS, et al. Functional coupling of mammalian receptors to the yeast mating pathway using novel yeast/mammalian G protein alpha-subunit

- chimeras. *Yeast*. 2000;16(1):11-22. doi:10.1002/(SICI)1097-0061(20000115)16:1<11::AID-YEA502>3.0.CO;2-K
71. Alvaro CG, Thorner J. Heterotrimeric G Protein-coupled Receptor Signaling in Yeast Mating Pheromone Response. *J Biol Chem*. 2016;291(15):7788-7795. doi:10.1074/jbc.R116.714980
 72. Minic J, Persuy M-A, Godel E, et al. Functional expression of olfactory receptors in yeast and development of a bioassay for odorant screening. *FEBS J*. 2005;272(2):524-537. doi:10.1111/j.1742-4658.2004.04494.x
 73. Lagane B, Gaibelet G, Meilhoc E, Masson JM, Cézanne L, Lopez A. Role of sterols in modulating the human mu-opioid receptor function in *Saccharomyces cerevisiae*. *J Biol Chem*. 2000;275(43):33197-33200. doi:10.1074/jbc.C000576200
 74. Kitson SM, Mullen W, Cogdell RJ, Bill RM, Fraser NJ. GPCR production in a novel yeast strain that makes cholesterol-like sterols. *Methods*. 2011;55(4):287-292. doi:https://doi.org/10.1016/j.ymeth.2011.09.023
 75. Gaibelet G, Meilhoc E, Riond J, et al. Nonselective coupling of the human mu-opioid receptor to multiple inhibitory G-protein isoforms. *Eur J Biochem*. 1999;261(2):517-523. doi:10.1046/j.1432-1327.1999.00301.x
 76. Souza CM, Schwabe TME, Pichler H, et al. A stable yeast strain efficiently producing cholesterol instead of ergosterol is functional for tryptophan uptake, but not weak organic acid resistance. *Metab Eng*. 2011;13(5):555-569. doi:https://doi.org/10.1016/j.ymben.2011.06.006
 77. Connor M, Christie MD. Opioid receptor signalling mechanisms. *Clin Exp Pharmacol Physiol*. 1999;26(7):493-499. doi:10.1046/j.1440-1681.1999.03049.x
 78. Koelle MR. A new family of G-protein regulators — the RGS proteins. *Curr Opin Cell Biol*. 1997;9(2):143-147. doi:https://doi.org/10.1016/S0955-0674(97)80055-5
 79. Nikko E, Pelham HRB. Arrestin-mediated endocytosis of yeast plasma membrane transporters. *Traffic*. 2009;10(12):1856-1867. doi:10.1111/j.1600-0854.2009.00990.x
 80. Ryan OW, Skerker JM, Maurer MJ, et al. Selection of chromosomal DNA libraries using a multiplex CRISPR system. *Elife*. 2014;3. doi:10.7554/eLife.03703
 81. Gietz RD, Schiestl RH. High-efficiency yeast transformation using the LiAc/SS carrier DNA/PEG method. *Nat Protoc*. 2007;2(1):31-34. doi:10.1038/nprot.2007.13
 82. Nes WD. Biosynthesis of cholesterol and other sterols. *Chem Rev*. 2011;111(10):6423-6451. doi:10.1021/cr200021m
 83. Nishi S, Nishino H, Ishibashi T. cDNA cloning of the mammalian sterol C5-desaturase and the expression in yeast mutant. *Biochim Biophys Acta*. 2000;1490(1-2):106-108. doi:10.1016/s0167-4781(99)00248-1
 84. Silve S, PH D, Labit-Lebouteiller C, et al. Emopamil-binding protein, a mammalian protein that binds a series of structurally diverse neuroprotective agents, exhibits delta8-delta7 sterol isomerase activity in yeast. *J Biol Chem*. 1996;271(37):22434-22440.
 85. Flagfeldt DB, Siewers V, Huang L, Nielsen J. Characterization of chromosomal integration sites for heterologous gene expression in *Saccharomyces cerevisiae*. *Yeast*. 2009;26(10):545-551. doi:10.1002/yea.1705
 86. Mikkelsen MD, Buron LD, Salomonsen B, et al. Microbial production of indolyglucosinolate through engineering of a multi-gene pathway in a versatile yeast expression platform. *Metab Eng*. 2012;14(2):104-111. doi:10.1016/j.ymben.2012.01.006
 87. Guan XL, Riezman I, Wenk MR, Riezman H. Yeast Lipid Analysis and Quantification by

- Mass Spectrometry. *Methods Enzymol.* 2010;470:369-391. doi:10.1016/S0076-6879(10)70015-X
88. Roberts CJ, Nelson B, Marton MJ, et al. Signaling and Circuitry of Multiple MAPK Pathways Revealed by a Matrix of Global Gene Expression Profiles. *Science (80-)*. 2000;287(5454):873 LP - 880. doi:10.1126/science.287.5454.873
 89. Slubowski CJ, Funk AD, Roesner JM, Paulissen SM, Huang LS. Plasmids for C-terminal tagging in *Saccharomyces cerevisiae* that contain improved GFP proteins, Envy and Ivy. *Yeast*. 2015;32(4):379-387. doi:10.1002/yea.3065
 90. Bourgeois L, Pyne ME, Martin VJJ. A Highly Characterized Synthetic Landing Pad System for Precise Multicopy Gene Integration in Yeast. *ACS Synth Biol*. 2018;7(11):2675-2685. doi:10.1021/acssynbio.8b00339
 91. Reider Apel A, d’Espaux L, Wehrs M, et al. A Cas9-based toolkit to program gene expression in *Saccharomyces cerevisiae*. *Nucleic Acids Res*. 2017;45(1):496-508. doi:10.1093/nar/gkw1023
 92. Black JW, Leff P. Operational models of pharmacological agonism. *Proc R Soc London Ser B Biol Sci*. 1983;220(1219):141-162. doi:10.1098/rspb.1983.0093
 93. Huang P, Chen C, Mague SD, Blendy JA, Liu-Chen L-Y. A common single nucleotide polymorphism A118G of the μ opioid receptor alters its N-glycosylation and protein stability. *Biochem J*. 2012;441(1):379-386. doi:10.1042/BJ20111050
 94. Letourneur F, Cosson P. Targeting to the Endoplasmic Reticulum in Yeast Cells by Determinants Present in Transmembrane Domains. *J Biol Chem* . 1998;273(50):33273-33278. doi:10.1074/jbc.273.50.33273
 95. Park SY, Guo X. Adaptor protein complexes and intracellular transport. *Biosci Rep*. 2014;34(4):e00123. doi:10.1042/BSR20140069
 96. Daboussi L, Costaguta G, Payne GS. Phosphoinositide-mediated clathrin adaptor progression at the trans-Golgi network. *Nat Cell Biol*. 2012;14(3):239-248. doi:10.1038/ncb2427
 97. Kirchhausen T. Three ways to make a vesicle. *Nat Rev Mol Cell Biol*. 2000;1(3):187-198. doi:10.1038/35043117
 98. Cowles CR, Odorizzi G, Payne GS, Emr SD. The AP-3 adaptor complex is essential for cargo-selective transport to the yeast vacuole. *Cell*. 1997;91(1):109-118. doi:10.1016/s0092-8674(01)80013-1
 99. Wright R, Basson M, D’Ari L, Rine J. Increased amounts of HMG-CoA reductase induce “karmellae”: a proliferation of stacked membrane pairs surrounding the yeast nucleus. *J Cell Biol*. 1988;107(1):101-114. doi:10.1083/jcb.107.1.101
 100. Huang KM, D’Hondt K, Riezman H, Lemmon SK. Clathrin functions in the absence of heterotetrameric adaptors and AP180-related proteins in yeast. *EMBO J*. 1999;18(14):3897-3908. doi:10.1093/emboj/18.14.3897
 101. Alvaro CG, O’Donnell AF, Prosser DC, et al. Specific α -arrestins negatively regulate *Saccharomyces cerevisiae* pheromone response by down-modulating the G-protein-coupled receptor Ste2. *Mol Cell Biol*. 2014;34(14):2660-2681. doi:10.1128/MCB.00230-14
 102. Savocco J, Nootens S, Afokpa W, et al. Yeast α -arrestin Art2 is the key regulator of ubiquitylation-dependent endocytosis of plasma membrane vitamin B1 transporters. *PLoS Biol*. 2019;17(10):e3000512. <https://doi.org/10.1371/journal.pbio.3000512>.
 103. Sørensen MA, Kurland CG, Pedersen S. Codon usage determines translation rate in

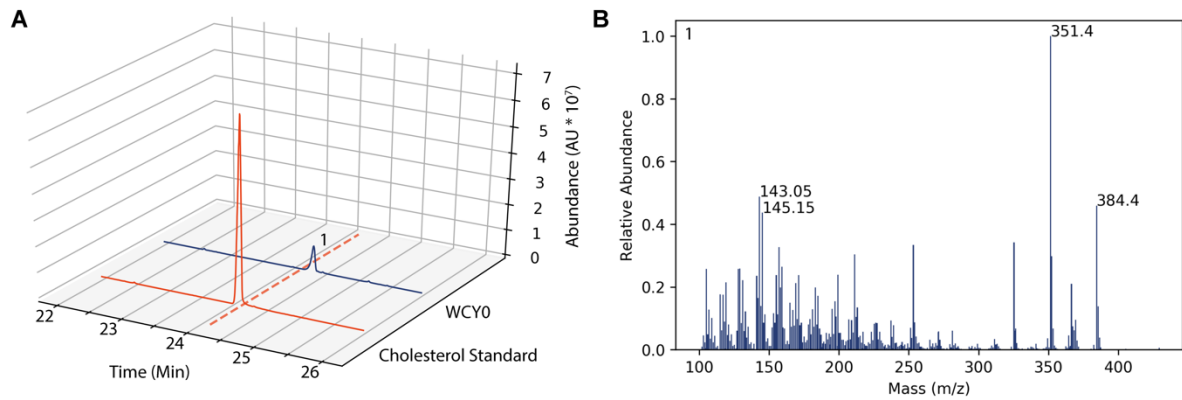
- Escherichia coli. *J Mol Biol.* 1989;207(2):365-377. doi:[https://doi.org/10.1016/0022-2836\(89\)90260-X](https://doi.org/10.1016/0022-2836(89)90260-X)
104. Purvis IJ, Bettany AJE, Santiago TC, et al. The efficiency of folding of some proteins is increased by controlled rates of translation in vivo: A hypothesis. *J Mol Biol.* 1987;193(2):413-417. doi:[https://doi.org/10.1016/0022-2836\(87\)90230-0](https://doi.org/10.1016/0022-2836(87)90230-0)
 105. Netzer WJ, Hartl FU. Recombination of protein domains facilitated by co-translational folding in eukaryotes. *Nature.* 1997;388(6640):343-349. doi:10.1038/41024
 106. Cabrita LD, Dobson CM, Christodoulou J. Protein folding on the ribosome. *Curr Opin Struct Biol.* 2010;20(1):33-45. doi:10.1016/j.sbi.2010.01.005
 107. Pechmann S, Frydman J. Evolutionary conservation of codon optimality reveals hidden signatures of cotranslational folding. *Nat Struct Mol Biol.* 2013;20(2):237-243. doi:10.1038/nsmb.2466
 108. Qu X, Wen J-D, Lancaster L, Noller HF, Bustamante C, Tinoco I. The ribosome uses two active mechanisms to unwind messenger RNA during translation. *Nature.* 2011;475(7354):118-121. doi:10.1038/nature10126
 109. Tao Y-X, Conn PM. Chaperoning G protein-coupled receptors: from cell biology to therapeutics. *Endocr Rev.* 2014;35(4):602-647. doi:10.1210/er.2013-1121
 110. Duan J, Wainwright MS, Comeron JM, et al. Synonymous mutations in the human dopamine receptor D2 (DRD2) affect mRNA stability and synthesis of the receptor. *Hum Mol Genet.* 2003;12(3):205-216. doi:10.1093/hmg/ddg055
 111. Clarke IV TF, Clark PL. Rare Codons Cluster. *PLoS One.* 2008;3(10):e3412. <https://doi.org/10.1371/journal.pone.0003412>.
 112. Schuldiner M, Collins SR, Thompson NJ, et al. Exploration of the Function and Organization of the Yeast Early Secretory Pathway through an Epistatic Miniarray Profile. *Cell.* 2005;123(3):507-519. doi:10.1016/j.cell.2005.08.031
 113. Virtanen P, Gommers R, Oliphant TE, et al. SciPy 1.0: fundamental algorithms for scientific computing in Python. *Nat Methods.* 2020;17(3):261-272. doi:10.1038/s41592-019-0686-2
 114. Kokkola T, Watson M-A, White J, Dowell S, Foord SM, Laitinen JT. Mutagenesis of Human Melanin Receptor Expressed in Yeast Reveals Domains Important for Receptor Function. *Biochem Biophys Res Commun.* 1998;249(2):531-536. doi:<https://doi.org/10.1006/bbrc.1998.9182>
 115. Huang W, Manglik A, Venkatakrishnan AJ, et al. Structural insights into μ -opioid receptor activation. *Nature.* 2015;524(7565):315-321. doi:10.1038/nature14886
 116. Venkatakrishnan AJ, Deupi X, Lebon G, et al. Diverse activation pathways in class A GPCRs converge near the G-protein-coupling region. *Nature.* 2016;536(7617):484-487. doi:10.1038/nature19107
 117. Venkatakrishnan AJ, Ma AK, Fonseca R, et al. Diverse GPCRs exhibit conserved water networks for stabilization and activation. *Proc Natl Acad Sci.* 2019;116(8):3288 LP - 3293. doi:10.1073/pnas.1809251116
 118. Ghanouni P, Schambye H, Seifert R, et al. The effect of pH on beta(2) adrenoceptor function. Evidence for protonation-dependent activation. *J Biol Chem.* 2000;275(5):3121-3127. doi:10.1074/jbc.275.5.3121
 119. Vetter I, Kapitzke D, Hermanussen S, Monteith GR, Cabot PJ. The effects of pH on beta-endorphin and morphine inhibition of calcium transients in dorsal root ganglion neurons. *J Pain.* 2006;7(7):488-499. doi:10.1016/j.jpain.2006.01.456

120. Mahalingam M, Martínez-Mayorga K, Brown MF, Vogel R. Two protonation switches control rhodopsin activation in membranes. *Proc Natl Acad Sci.* 2008;105(46):17795 LP - 17800. doi:10.1073/pnas.0804541105
121. Ruusuvauro E, Kaila K. Carbonic Anhydrases and Brain pH in the Control of Neuronal Excitability BT - Carbonic Anhydrase: Mechanism, Regulation, Links to Disease, and Industrial Applications. In: Frost SC, McKenna R, eds. Dordrecht: Springer Netherlands; 2014:271-290. doi:10.1007/978-94-007-7359-2_14
122. Shaw WM, Yamauchi H, Mead J, et al. Engineering a Model Cell for Rational Tuning of GPCR Signaling. *Cell.* 2019;177(3):782-796.e27. doi:10.1016/j.cell.2019.02.023
123. Ross EM, Wilkie TM. GTPase-Activating Proteins for Heterotrimeric G Proteins: Regulators of G Protein Signaling (RGS) and RGS-Like Proteins. *Annu Rev Biochem.* 2000;69(1):795-827. doi:10.1146/annurev.biochem.69.1.795
124. Rogers JK, Taylor ND, Church GM. Biosensor-based engineering of biosynthetic pathways. *Curr Opin Biotechnol.* 2016;42:84-91. doi:https://doi.org/10.1016/j.copbio.2016.03.005
125. Di Roberto RB, Chang B, Trusina A, Peisajovich SG. Evolution of a G protein-coupled receptor response by mutations in regulatory network interactions. *Nat Commun.* 2016;7:12344. doi:10.1038/ncomms12344
126. Schütz M, Schöppe J, Sedláč E, et al. Directed evolution of G protein-coupled receptors in yeast for higher functional production in eukaryotic expression hosts. *Sci Rep.* 2016;6(1):21508. doi:10.1038/srep21508
127. Sarkar CA, Dodevski I, Kenig M, et al. Directed evolution of a G protein-coupled receptor for expression, stability, and binding selectivity. *Proc Natl Acad Sci.* 2008;105(39):14808 LP - 14813. doi:10.1073/pnas.0803103105
128. Laughlin SB, Sejnowski TJ. Communication in neuronal networks. *Science.* 2003;301(5641):1870-1874. doi:10.1126/science.1089662
129. Regot S, Macia J, Conde N, et al. Distributed biological computation with multicellular engineered networks. *Nature.* 2011;469(7329):207-211. doi:10.1038/nature09679
130. Billerbeck S, Brisbois J, Agmon N, et al. A scalable peptide-GPCR language for engineering multicellular communication. *Nat Commun.* 2018;9(1):5057. doi:10.1038/s41467-018-07610-2
131. Hanson MA, Cherezov V, Griffith MT, et al. A specific cholesterol binding site is established by the 2.8 Å structure of the human beta2-adrenergic receptor. *Structure.* 2008;16(6):897-905. doi:10.1016/j.str.2008.05.001
132. Klein U, Gimpl G, Fahrenholz F. Alteration of the Myometrial Plasma Membrane Cholesterol Content with .beta.-Cyclodextrin Modulates the Binding Affinity of the Oxytocin Receptor. *Biochemistry.* 1995;34(42):13784-13793. doi:10.1021/bi00042a009
133. Prabhu A V, Luu W, Li D, Sharpe LJ, Brown AJ. DHCR7: A vital enzyme switch between cholesterol and vitamin D production. *Prog Lipid Res.* 2016;64:138-151. doi:https://doi.org/10.1016/j.plipres.2016.09.003
134. Lock E-J, Waagbø R, Wendelaar Bonga S, Flik G. The significance of vitamin D for fish: a review. *Aquac Nutr.* 2010;16(1):100-116. doi:10.1111/j.1365-2095.2009.00722.x
135. Hu Z, He B, Ma L, Sun Y, Niu Y, Zeng B. Recent Advances in Ergosterol Biosynthesis and Regulation Mechanisms in *Saccharomyces cerevisiae*. *Indian J Microbiol.* 2017;57(3):270-277. doi:10.1007/s12088-017-0657-1
136. Thomas DS, Hossack JA, Rose AH. Plasma-Membrane lipid composition and ethanol

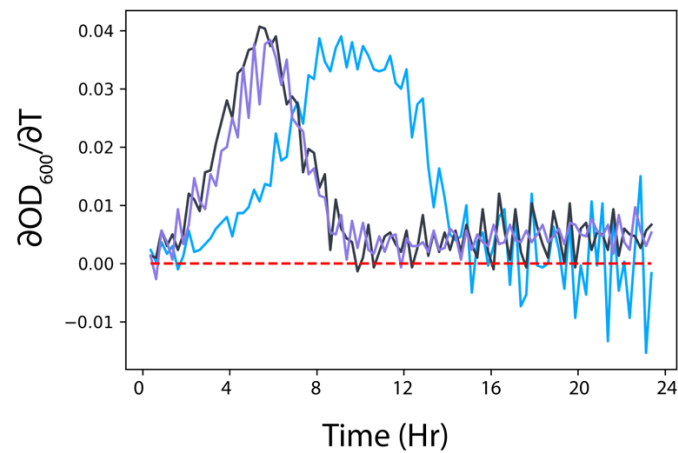
- tolerance in *Saccharomyces cerevisiae*. *Arch Microbiol.* 1978;117(3):239-245. doi:10.1007/BF00738541
137. Henderson CM, Block DE. Examining the role of membrane lipid composition in determining the ethanol tolerance of *Saccharomyces cerevisiae*. *Appl Environ Microbiol.* 2014;80(10):2966-2972. doi:10.1128/AEM.04151-13
 138. Gaber RF, Coppole DM, Kennedy BK, Vidal M, Bard M. The yeast gene ERG6 is required for normal membrane function but is not essential for biosynthesis of the cell-cycle-sparking sterol. *Mol Cell Biol.* 1989;9(8):3447-3456. doi:10.1128/mcb.9.8.3447
 139. Wolin SL, Walter P. Discrete nascent chain lengths are required for the insertion of presecretory proteins into microsomal membranes. *J Cell Biol.* 1993;121(6):1211-1219. doi:10.1083/jcb.121.6.1211
 140. Faure G, Ogurtsov AY, Shabalina SA, Koonin E V. Role of mRNA structure in the control of protein folding. *Nucleic Acids Res.* 2016;44(22):10898-10911. doi:10.1093/nar/gkw671
 141. Davis ME, Akera T, Brody TM, Watson L. Opiate receptor: cooperativity of binding observed in brain slices. *Proc Natl Acad Sci U S A.* 1977;74(12):5764-5766. doi:10.1073/pnas.74.12.5764
 142. Maderspach K, Solomonia R. Glial and neuronal opioid receptors: apparent positive cooperativity observed in intact cultured cells. *Brain Res.* 1988;441(1):41-47. doi:https://doi.org/10.1016/0006-8993(88)91381-9
 143. Chabre M, Deterre P, Antonny B. The apparent cooperativity of some GPCRs does not necessarily imply dimerization. *Trends Pharmacol Sci.* 2009;30(4):182-187. doi:https://doi.org/10.1016/j.tips.2009.01.003
 144. Petäjä-Repo UE, Hogue M, Laperrière A, Walker P, Bouvier M. Export from the Endoplasmic Reticulum Represents the Limiting Step in the Maturation and Cell Surface Expression of the Human δ Opioid Receptor. *J Biol Chem.* 2000;275(18):13727-13736. <http://www.jbc.org/content/275/18/13727.abstract>.
 145. Angel TE, Chance MR, Palczewski K. Conserved waters mediate structural and functional activation of family A (rhodopsin-like) G protein-coupled receptors. *Proc Natl Acad Sci.* 2009;106(21):8555 LP - 8560. doi:10.1073/pnas.0903545106
 146. Ballesteros JA, Weinstein H. [19] Integrated methods for the construction of three-dimensional models and computational probing of structure-function relations in G protein-coupled receptors. In: Sealfon SCBT-M in N, ed. *Receptor Molecular Biology*. Vol 25. Academic Press; 1995:366-428. doi:https://doi.org/10.1016/S1043-9471(05)80049-7
 147. Koehl A, Hu H, Maeda S, et al. Structure of the μ -opioid receptor–Gi protein complex. *Nature.* 2018;558(7711):547-552. doi:10.1038/s41586-018-0219-7
 148. Meyer J, Del Vecchio G, Seitz V, Massaly N, Stein C. Modulation of μ -opioid receptor activation by acidic pH is dependent on ligand structure and an ionizable amino acid residue. *Br J Pharmacol.* 2019;176(23):4510-4520. doi:10.1111/bph.14810
 149. Li S, Hong M. Protonation, tautomerization, and rotameric structure of histidine: a comprehensive study by magic-angle-spinning solid-state NMR. *J Am Chem Soc.* 2011;133(5):1534-1544. doi:10.1021/ja108943n
 150. McPherson J, Rivero G, Baptist M, et al. μ -opioid receptors: correlation of agonist efficacy for signalling with ability to activate internalization. *Mol Pharmacol.* 2010;78(4):756-766. doi:10.1124/mol.110.066613

151. Williams JT, Ingram SL, Henderson G, et al. Regulation of μ -opioid receptors: desensitization, phosphorylation, internalization, and tolerance. *Pharmacol Rev.* 2013;65(1):223-254. doi:10.1124/pr.112.005942

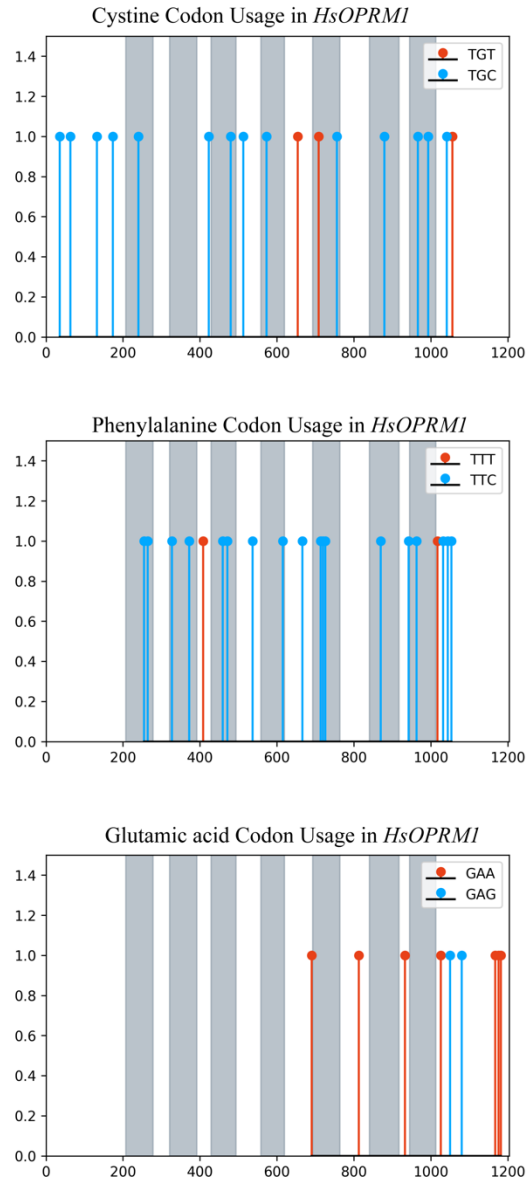
Supplemental Data



Supplemental Figure 1. (A) GC-MS Chromatograph of WCY0 total ion count between 22 and 26 minutes. WCY0 peak was distinct from cholesterol standard (B) Extracted Mass Spectrum of peak 1 from A. Comparison of spectra by the NIST database identified 7-dehydrocholesterol with a 29.0% match.



Supplemental Figure 2. Growth rate for BY4741 (black), WCY1 (blue) and BBY1580 (purple). Dashed line corresponds to $\partial OD_{600} / \partial T = 0$.



Supplemental Figure 3. Position of cysteine, phenylalanine and glutamic codons in *HsOPRM1*. Cysteine, phenylalanine and glutamic acid codons all showed deviation from expected codon usage in *HsOPRM1*. Shaded regions represent transmembrane helices.

